Effective holographic models for QCD: Glueball spectrum and trace anomaly

Alfonso Ballon-Bayona,[1,*] Henrique Boschi-Filho,[2,†] Luis A. H. Mamani,[3,‡] Alex S. Miranda,[4,§] and Vilson T. Zanchin[3,‖]

[1]*Instituto de Física Teórica, Universidade Estadual Paulista, Rua Dr. Bento Teobaldo Ferraz, 271—Bloco II, 01140-070 São Paulo, São Paulo, Brazil*
[2]*Instituto de Física, Universidade Federal do Rio de Janeiro, Caixa Postal 68528, Rio de Janeiro 21941-972, Brazil*
[3]*Centro de Ciências Naturais e Humanas, Universidade Federal do ABC, Rua Santa Adélia 166, 09210-170 Santo André, São Paulo, Brazil*
[4]*Laboratório de Astrofísica Teórica e Observacional, Departamento de Ciências Exatas e Tecnológicas, Universidade Estadual de Santa Cruz, 45650-000 Ilhéus, Bahia, Brazil*

(Received 4 December 2017; published 1 February 2018)

We investigate effective holographic models for QCD arising from five-dimensional dilaton gravity. The models are characterized by a dilaton with a mass term in the UV, dual to a CFT deformation by a relevant operator, and quadratic in the IR. The UV constraint leads to the explicit breaking of conformal symmetry, whereas the IR constraint guarantees linear confinement. We propose semianalytic interpolations between the UV and the IR and obtain a spectrum for scalar and tensor glueballs consistent with lattice QCD data. We use the glueball spectrum as a physical constraint to find the evolution of the model parameters as the mass term goes to 0. Finally, we reproduce the universal result for the trace anomaly of deformed CFTs and propose a dictionary between this result and the QCD trace anomaly. A nontrivial consequence of this dictionary is the emergence of a β function similar to the two-loop perturbative QCD result.

DOI: 10.1103/PhysRevD.97.046001

I. INTRODUCTION

QCD is probably the most striking example of conformal symmetry breaking in a quantum field theory. In QCD conformal symmetry is broken already in the UV by a negative β function (asymptotic freedom) that, at the same time, leads to strong coupling and confinement in the IR. Despite the huge success of perturbative QCD in describing hard scattering processes, basic QCD features in the IR, such as the hadronic spectrum or chiral symmetry breaking, require the development of nonperturbative methods. The most well-established nonperturbative approach consists of Monte Carlo simulations for QCD on a lattice. The so-called lattice QCD is very successful in describing static properties such as the hadronic spectrum and thermodynamic properties of the quark-gluon plasma. However, real-time dynamics usually demands the development of other nonperturbative methods.

Holographic QCD provides a nonperturbative description of real-time QCD dynamics in terms of the dynamics of a five-dimensional gravitational (string) theory. In the so-called bottom-up approach, the dictionary arising from the AdS/CFT correspondence is used to build a set of five-dimensional fields dual to the QCD operators responsible for describing the QCD vacuum. In the large-N_c limit one focuses on the stress-energy tensor $T^{\mu\nu}$ of the gluon field, as well as on the scalar operator $\mathrm{Tr}F^2$ responsible for the gluon condensate and the QCD scale anomaly, i.e. $T^{\mu}{}_{\mu} \sim \mathrm{Tr}F^2$ [1]. In holography the operators $T^{\mu\nu}$ and $\mathrm{Tr}F^2$ couple to a five-dimensional metric and scalar field (the dilaton), respectively. The dynamics of the metric and dilaton fields is determined by the equations of the dilaton-gravity theory, and the dilaton potential contains a negative cosmological constant leading to AdS geometry in the UV. Since Lorentz invariance is not broken by the QCD vacuum, in holographic QCD one takes a conformally flat metric with a warp factor A depending solely on the radial coordinate z. Then a nonconstant dilaton $\Phi(z)$ leads to a deformation of the anti–de Sitter (AdS) spacetime geometry. This is the holographic realization of conformal

*aballonb@ift.unesp.br
†boschi@if.ufrj.br
‡luis.mamani@ufabc.edu.br
§asmiranda@uesc.br
‖zanchin@ufabc.edu.br

symmetry breaking in large-N_c QCD. Assuming that $\Phi(z)$ couples directly to the operator $\mathrm{Tr}F^2$ at the boundary one would expect, according to the AdS/CFT dictionary, $\Phi(z)$ is to behave as $\phi_0 + Gz^4$ near the boundary. This assumption, however, was shown not to be consistent with the glueball spectrum [2], because in that case conformal symmetry is spontaneously broken, leading to a zero mode in the spectrum (a Nambu-Goldstone boson).

There are two possible solutions to this problem. The first one consists of making the dilaton potential compatible with asymptotic freedom in the UV, as advocated in [2]. This scenario was realized in the so-called improved holographic QCD (IHQCD) models [3,4], proposed by Gursoy *et al.* These authors also found the right physical constraint for the dilaton in the IR: a confining background, which corresponds to a quadratic dilaton for large z and leads to an approximate linear glueball spectrum. Interestingly, that behavior had already been anticipated in the soft-wall model [5] from the analysis of the meson spectrum. The second solution consists of introducing a mass term for the dilaton potential in the UV. In this case the near-boundary behavior of the dilaton field becomes $\phi_0 z^\epsilon + Gz^{4-\epsilon}$, with ϵ related to the dilaton mass M by $M^2\ell^2 = -\epsilon(4-\epsilon)$, where ℓ is the AdS radius. This UV asymptotics was proposed by Gubser *et al.* in [6,7], within the context of finite-temperature holographic QCD as a model for describing the equation of state of a nonconformal plasma through a five-dimensional black hole. In [6,7] the parameter ϵ was interpreted in terms of the anomalous dimension of the operator $\mathrm{Tr}F^2$.

Inspired by the seminal works [3,4] and [6,7], we investigate in this paper a family of holographic QCD backgrounds where the IR is driven by linear confinement and the UV, although asymptotically AdS, is deformed by a dilaton field with nonzero mass. We interpret the dilaton mass term in the UV as the holographic description of a CFT deformation $\delta\mathcal{L} = \phi_0\mathcal{O}$, where $\mathcal{O}$ is a relevant operator and ϕ_0 is the corresponding coupling. This interpretation was advocated in [6,7] and is consistent with previous studies in holographic renormalization [8,9]. The main motivation for this work is to understand how holography realizes conformal symmetry breaking in the UV without introducing explicitly the β function of large-N_c QCD. Our guide in this investigation is the spectrum of scalar and tensor glueballs, because it allows us to fix the source and the vacuum expectation value (VEV) coefficients in the near-boundary expansion.[1] As in Refs. [6,7], we assume that the CFT deformation takes place at a UV energy scale μ^*. However, although $4-\epsilon$ is indeed the conformal dimension of the operator $\mathcal{O}$ (responsible for the CFT deformation), the relation between $\mathcal{O}$ and the QCD operator $\mathrm{Tr}F^2$ is not direct. Therefore, we do not interpret the parameter ϵ as the anomalous dimension ϵ_{an} of the operator $\mathrm{Tr}F^2$, as was advocated in [6,7]. We, however, propose a relation between these two quantities.

We show in this work that for arbitrary values of ϵ, in the range $0.001 < \epsilon < 0.1$, it is always possible to reproduce the spectrum of scalar and tensor glueballs obtained in lattice QCD. This is achieved by using the first two scalar glueball masses as a physical criterion to fix the source and VEV coefficients, ϕ_0 and G, respectively, for each value of ϵ. We find that the evolution of these parameters as functions of ϵ admits simple fits that allow us to predict their behavior in the $\epsilon \to 0$ limit (where the dilaton becomes massless). On the other hand, from the analysis of the vacuum energy density $\langle T^{00}\rangle$ and the VEV of $\mathcal{O}$ we calculate the corresponding trace anomaly $\langle T^\mu{}_\mu\rangle = -\epsilon\phi_0\langle O\rangle$, which is consistent with the general result of deformed CFTs [9,14]. We suggest a reinterpretation of this result in terms of the QCD trace anomaly, which in turn suggests a dictionary for the parameters ϕ_0 and ϵ.

Our approach is quite different from the one considered in [3,4], where the four-dimensional theory does not have a UV cutoff and the dilaton potential is built to reproduce the two-loop perturbative β function of large-N_c QCD (asymptotic freedom). It is not clear, however, how the holographic map between the energy μ and the warp factor $A(z)$, proposed in [3,4], should be modified in our case in order to accommodate the energy cutoff μ^*. In recent works [15,16], a massive term for the dilaton in the UV was interpreted as the dual of a CFT deformation by a nearly marginal operator and the corresponding renormalization group (RG) flow was investigated (see also [17]). Our results, however, support the interpretation of the CFT deformation $\delta\mathcal{L} = \phi_0\mathcal{O}$ in terms of the large-N_c Yang-Mills Lagrangian. In some sense this is a reinterpretation of the RG flow in holographic QCD where now the operator $\mathrm{Tr}F^2$ is interpreted as the source of a nontrivial β function. This may also shed some light on the origin of the dilaton potentials considered in holographic QCD models without relying on a stringy top-down approach.

This paper is organized as follows. In Sec. II we review the holographic QCD models arising from five-dimensional dilaton-gravity theory, with focus on the linearized equations that lead to the glueball spectrum. Then, in Sec. III, we describe the physical constraints in the UV and IR, compatible with explicit conformal symmetry breaking and linear confinement, and present two interpolations where the dilaton admits an analytic form. In Sec. IV we find a spectrum for scalar and tensor glueballs compatible with lattice QCD data and describe how the model parameters evolve with the conformal dimension ϵ. In Sec. V we calculate the trace anomaly for our model, which agrees

[1]This approach is similar to the one used in the holographic model for chiral symmetry breaking [10,11] where the quark masses and chiral condensates are fixed by the meson masses and decay constants. See also [12,13].

with the general expectation of deformed CFTs and compare this result with the QCD scale anomaly. We finish this paper with our conclusions and two appendixes. Appendix A describes massless scalar modes in holographic QCD. In Appendix B we present two holographic QCD models where the warp factor admits an analytic form.

II. REVIEW OF HOLOGRAPHIC QCD

In this section we review the holographic QCD (HQCD) backgrounds in a bottom-up approach, which makes use of the field/operator correspondence unveiled by the AdS/CFT correspondence. In order to describe the large-N_c QCD vacuum the focus is on the stress-energy tensor $T^{\mu\nu}$ as well as the Yang-Mills Lagrangian operator $\mathrm{Tr}F^2$. The former couples to a five-dimensional metric g_{mn} and the latter couples to the scalar dilaton field Φ. Then the natural five-dimensional framework is the dilaton-gravity theory, where besides the Einstein-Hilbert action one considers a dilaton kinetic term and a dilaton potential.

First we exploit the fact that HQCD backgrounds are conformally flat and map the perturbed metric to linearized gravity around the Minkowski spacetime. Then we briefly review the general features of the models proposed in [3,4], also known as IHQCD. We finish the section with a full description of the linearized dilaton-gravity equations leading to the glueball spectrum.

A. Ricci tensor in HQCD backgrounds

Consider a Weyl transformation for a five-dimensional metric,

$$g_{mn} = e^{2A(x)}\bar{g}_{mn}. \tag{1}$$

We take the transformation (1) as a field redefinition for the metric, or as an ansatz for the background spacetime.[2] In holography the five-dimensional coordinates x^m of the bulk spacetime decompose as (x^μ, z) where x^μ are the four-dimensional coordinates associated with the field theory at the boundary and z is the bulk radial coordinate.

The metrics g_{mn} and $\bar{g}_{mn}$ include also the fluctuations around the unperturbed background, and so they admit the expansions

$$\bar{g}_{mn} = \bar{g}^{(0)}_{mn} + \bar{g}^{(1)}_{mn} + \cdots, \quad g_{mn} = g^{(0)}_{mn} + g^{(1)}_{mn} + \cdots, \tag{2}$$

where we take $\bar{g}^{(0)}_{mn}$ as the metric associated with a reference background. Analogously, the Christoffel symbols $\Gamma^p_{mn} = \frac{1}{2}g^{pq}(\partial_m g_{qn} + \partial_n g_{qm} - \partial_q g_{mn})$ and the Ricci tensor $R_{mn} \equiv R^p{}_{mpn} = \partial_p\Gamma^p_{nm} - \partial_n\Gamma^p_{pm} + \Gamma^p_{pq}\Gamma^q_{nm} - \Gamma^p_{nq}\Gamma^q_{pm}$ also admit the expansions

$$\begin{aligned}
\bar{\Gamma}^p_{mn} &= \bar{\Gamma}^{p(0)}_{mn} + \bar{\Gamma}^{p(1)}_{mn} + \cdots, \qquad \Gamma^p_{mn} = \Gamma^{p(0)}_{mn} + \Gamma^{p(1)}_{mn} + \cdots, \\
\bar{R}_{mn} &= \bar{R}^{(0)}_{mn} + \bar{R}^{(1)}_{mn} + \cdots, \qquad R_{mn} = R^{(0)}_{mn} + R^{(1)}_{mn} + \cdots.
\end{aligned} \tag{3}$$

The Ricci tensor transforms under (1) as

$$\begin{aligned}
R_{mn} = \bar{R}_{mn} &- 3[\partial_m\partial_n A - \bar{\Gamma}^p_{mn}\partial_p A] + 3\partial_m A\partial_n A \\
&- \bar{g}_{mn}\bar{g}^{pq}[\partial_p\partial_q A - \bar{\Gamma}^r_{pq}\partial_r A + 3\partial_p A\partial_q A].
\end{aligned} \tag{4}$$

In HQCD we are interested in the case where the reference background is flat, i.e.

$$\bar{g}^{(0)}_{mn} = \eta_{mn}, \qquad \bar{\Gamma}^{p(0)}_{mn} = 0, \qquad \bar{R}^{(0)}_{mn} = 0, \tag{5}$$

and we take the warp factor A as a function of the radial coordinate only, i.e. $A = A(z)$, so that four-dimensional Poincaré symmetry, associated with the coordinates x^μ, is preserved. Then at 0th order the Ricci tensor of the dual metric takes the form

$$R^{(0)}_{mn} = -3\partial_m\partial_n A + 3\partial_m A\partial_n A - \eta_{mn}(A'' + 3A'^2), \tag{6}$$

where $'$ means d/dz. Projecting out the Ricci tensor we obtain the components

$$R^{(0)}_{zz} = -4A'', \quad R^{(0)}_{z\mu} = 0, \quad R^{(0)}_{\mu\nu} = -\eta_{\mu\nu}(A'' + 3A'^2), \tag{7}$$

and the 0th order Ricci scalar $R \equiv g^{mn}R_{mn}$ takes the form

$$R^{(0)} = -e^{-2A}(8A'' + 12A'^2). \tag{8}$$

On the other hand, the reference metric at first order is that of linearized gravity around flat space, i.e.

$$\begin{aligned}
\bar{g}^{(1)}_{mn} &= h_{mn}, \\
\bar{\Gamma}^{p(1)}_{mn} &= \partial_{(m}h_{n)}{}^p - \frac{1}{2}\partial^p h_{mn}, \\
\bar{R}^{(1)}_{mn} &= \partial_p\partial_{(m}h_{n)}{}^p - \frac{1}{2}\partial_p\partial^p h_{mn} - \frac{1}{2}\partial_m\partial_n h_p{}^p,
\end{aligned} \tag{9}$$

where the parentheses around the indices denote symmetrization, $V_{(mn)} \equiv (V_{mn} + V_{nm})/2$, and the indices of h_{mn} are raised (lowered) using the Minkowski metric η^{mn} (η_{mn}).

Expanding both sides of (4), we find that the first order perturbations of the Ricci tensor can be written as

$$\begin{aligned}
R^{(1)}_{mn} = \bar{R}^{(1)}_{mn} &+ 3A'\bar{\Gamma}^{z(1)}_{mn} + (A'' + 3A'^2)(h_{zz}\eta_{mn} - h_{mn}) \\
&+ A'\eta^{pq}\bar{\Gamma}^{z(1)}_{pq}\eta_{mn}.
\end{aligned} \tag{10}$$

Decomposing the tensor of linearized gravity h_{mn} as $(h_{zz}, h_{z\mu}, h_{\mu\nu})$ and defining $h_{zz} \equiv 2\phi$ and $h_{z\mu} \equiv \mathcal{A}_\mu$, we can project out the Ricci tensor (10) and find the following components:

[2]This is in contrast with the Weyl transformations used in string theory where the conformal factor is also a field.

$$
\begin{aligned}
R^{(1)}_{zz} &= [\partial_z + A']\left(\partial_\mu \mathcal{A}^\mu - \frac{1}{2}h'\right) + 4A'\phi' - \Box\phi;\\
R^{(1)}_{z\mu} &= \frac{1}{2}\partial_\nu h'^{\nu}_{\mu} - \frac{1}{2}\partial_\mu h' + \frac{1}{2}\partial_\nu \mathcal{F}^{\nu}_{\mu} + 3A'\partial_\mu\phi\\
&\quad - (A'' + 3A'^2)\mathcal{A}_\mu;\\
R^{(1)}_{\mu\nu} &= [\partial_z + 3A']\partial_{(\mu}\mathcal{A}_{\nu)} - \frac{1}{2}[\partial_z^2 + 3A'\partial_z + \Box]h_{\mu\nu}\\
&\quad + \partial_\rho\partial_{(\mu}h^{\rho}_{\nu)} - \frac{1}{2}\partial_\mu\partial_\nu(2\phi + h)\\
&\quad + \frac{1}{2}A'[2\phi' - h' + 2\partial_\rho\mathcal{A}^\rho]\eta_{\mu\nu}\\
&\quad + (A'' + 3A'^2)[2\phi\eta_{\mu\nu} - h_{\mu\nu}],
\end{aligned}
\tag{11}
$$

where $\Box \equiv \partial_\mu\partial^\mu$ is the d'Alembertian operator in the boundary spacetime, the scalar h is defined by the trace $h \equiv h^\mu{}_\mu$ and $\mathcal{F}_{\mu\nu} \equiv \partial_\mu\mathcal{A}_\nu - \partial_\nu\mathcal{A}_\mu$ is the field strength associated with the vector $\mathcal{A}_\mu$.

B. HQCD backgrounds from dilaton gravity

The goal of holographic QCD is to find the gravity (string) dual of QCD in the large-N_c limit. This is motivated by the 't Hooft planar limit [18] and the AdS/CFT correspondence [19–21]. QCD is, on the one hand, well approximated by a CFT in the UV and, on the other hand, confining in the IR. These facts suggest that the holographic dual spacetime should be AdS near the boundary. Far from the boundary, it should be such that dual probe fields (and strings) living in that five-dimensional background reproduce confinement and the four-dimensional hadronic physics. In the pioneer work of [3,4], a very general family of HQCD backgrounds was proposed and, based on the work of [22], a universal IR criterion for confinement was found. Moreover, the requirement of linear Regge trajectories led the authors of [4] to conclude that a quadratic dilaton field was necessary in the IR. This supports the early work of [5], where a quadratic dilaton was proposed on the basis of the meson spectrum, the so-called soft-wall model.

In this subsection, we briefly review the HQCD backgrounds proposed in [3,4] focusing on the IR physics. In the next subsection, we describe the scalar and gravitational perturbations that lead to the Schrödinger equations associated with the glueball spectrum.

In the HQCD approach, we start with a five-dimensional dilaton-gravity action of the form

$$
S = M_p^3 N_c^2 \int d^5x\sqrt{-g}[R + \mathcal{L}_\Phi], \tag{12}
$$

where M_p is the five-dimensional Planck scale, N_c is the number of colors, and the dilaton Lagrangian has a kinetic term and a potential,

$$
\mathcal{L}_\Phi = -\frac{4}{3}g^{mn}\partial_m\Phi\partial_n\Phi + V(\Phi). \tag{13}
$$

Variating the action (12) with respect to Φ and the metric g_{mn}, we obtain the dilaton-gravity equations

$$
R_{mn} - \frac{1}{2}g_{mn}R = \frac{1}{2M_p^3N_c^2}T_{mn}, \tag{14}
$$

$$
\frac{4}{3}\nabla^2\Phi + \frac{1}{2}\frac{dV}{d\Phi} = 0, \tag{15}
$$

where ∇^2 is the Laplacian operator[3] and we have defined an energy-momentum tensor T_{mn} for the dilaton field,

$$
T_{mn} \equiv M_p^3N_c^2\left[\frac{8}{3}\partial_m\Phi\partial_n\Phi + g_{mn}\mathcal{L}_\Phi\right]. \tag{16}
$$

It is also convenient to write the Einstein equations (14) in the Ricci form,

$$
R_{mn} = \frac{4}{3}\partial_m\Phi\partial_n\Phi - \frac{1}{3}g_{mn}V. \tag{17}
$$

The HQCD backgrounds correspond to solutions for the dilaton-gravity equations of the form

$$
ds^2 = e^{2A(z)}[dz^2 + \eta_{\mu\nu}dx^\mu dx^\nu], \qquad \Phi = \Phi(z). \tag{18}
$$

The warp factor $A(z)$ and dilaton $\Phi(z)$ are usually mapped to the energy scale and coupling of the dual four-dimensional theory. Using (7) and the definition of the scalar Laplacian ∇^2, the dilaton-gravity equations (15) and (17) take the form

$$
\begin{aligned}
12A'' + 4\Phi'^2 &= e^{2A}V,\\
3A'' + 9A'^2 &= e^{2A}V,\\
\frac{8}{3}[\partial_z + 3A']\Phi' &= -e^{2A}\frac{dV}{d\Phi}.
\end{aligned}
\tag{19}
$$

The last equation in (19) can be obtained from the first two, which in turn can be rewritten as

$$
\begin{aligned}
A'^2 - A'' &= \frac{4}{9}\Phi'^2,\\
3A'^2 + A'' &= \frac{1}{3}e^{2A}V.
\end{aligned}
\tag{20}
$$

At this point it is very convenient to define the quantity

$$
\zeta(z) \equiv \exp[-A(z)], \tag{21}
$$

[3]The Laplacian operator ∇^2 applied to a scalar function f is given by $\nabla^2 f = \frac{1}{\sqrt{-g}}\partial_m(\sqrt{-g}g^{mn}\partial_n f)$.

so that the first equation in (20) takes a linear form in ζ,

$$\zeta'' - \frac{4}{9}\Phi'^2\zeta = 0. \tag{22}$$

The Schrödinger form of this equation is useful to understand the AdS deformation due to a nonconstant dilaton, which is the dual of a conformal symmetry breaking. In the case of a constant dilaton, the interesting solution for the holography is $\zeta = z/\ell$, corresponding to the usual AdS spacetime with curvature radius ℓ. In this paper we describe how the presence of dilaton mass, associated with a CFT deformation, leads to an explicit breaking of conformal symmetry and gives a reasonable glueball spectrum. Note from Eq. (22) that $\zeta'' \geq 0$ for all values of z. AdS asymptotics implies that $\zeta'(0) = 1/\ell$ so we conclude that $\zeta' \geq 1/\ell$.[4]

Following Ref. [4] we write the equations (20) as a system of first order differential equations

$$\zeta\Phi' = \frac{dW}{d\Phi}, \qquad \zeta' = \frac{4}{9}W,$$
$$V = -\frac{4}{3}\left(\frac{dW}{d\Phi}\right)^2 + \frac{64}{27}W^2, \tag{23}$$

where $W = W(\Phi)$ is the superpotential associated with the dilaton-gravity dynamics. Another useful quantity is the field X defined by the relations

$$X \equiv \frac{1}{3}\frac{d\Phi}{dA} = -\frac{1}{3}\frac{\zeta\Phi'}{\zeta'} = -\frac{3}{4}\frac{d\log W}{d\Phi}. \tag{24}$$

This field can be interpreted as a bulk beta function $X \sim \beta_\Phi$ describing the evolution of the dilaton Φ with the warp factor A. In the next subsection we describe how this field appears in the Schrödinger equation associated with scalar glueballs. In [3,4] the authors proposed a dictionary that maps the bulk field X to the β function of the four-dimensional dual theory. In our work the CFT deformation in the UV implies the existence of a cutoff μ^* in the energy scale of the four-dimensional theory. This feature suggests a departure from the map proposed in [3,4] so we take X as a pure bulk field. In particular, we see that while X goes to 0 as we approach the boundary the dual β function is still finite.

We finish this subsection describing the confining constraint found in [4]. The discussion takes place in the string frame, where the metric is given by

$$ds^2 = e^{2A_s(z)}[dz^2 + \eta_{\mu\nu}dx^\mu dx^\nu], \tag{25}$$

and the string-frame warp factor is related to the Einstein-frame warp factor by

$$A_s(z) = A(z) + \frac{2}{3}\Phi(z). \tag{26}$$

Consider a static string living in the spacetime (25), with end points attached to the boundary and separated by a distance L in one of the boundary directions. As shown in [22], inspired by [23], this problem maps to a rectangular Wilson loop describing in the large-L limit the potential energy of a heavy quark-antiquark pair. Solving the Nambu-Goto equations one finds that in the large-L limit the energy of the static string takes the form

$$E(L) = \mu_s f(z_*)L + \cdots, \tag{27}$$

where μ_s is the fundamental string tension, $f(z) = \exp(2A_s)$, and z_* is the point where $f(z)$ has a minimum and the dots represent subleading terms in the large-L limit. Following Ref. [22], the energy (27) maps to the quark-antiquark potential and confinement is achieved for $f(z_*) > 0$. In this case, the quantity $\mu_s f(z_*)$ is identified with the confining string tension σ.

Thus we conclude that confining backgrounds are those where the function $f(z) = \exp(2A_s)$ has a nonzero minimum. Since we always consider backgrounds that are asymptotically AdS we have that $f(z) \to \infty$ in the UV ($z \to 0$). We are interested in backgrounds where $0 < z < \infty$ so we conclude that in the IR $f(z \to \infty) > 0$ to guarantee confinement. Taking a power ansatz for the dilaton $\Phi(z) = Cz^\alpha$ we find from (20) that at large z

$$A(z) = -\frac{2}{3}\Phi(z) + \frac{1}{2}\log|\Phi'(z)| + \cdots, \tag{28}$$

so that

$$A_s(z) = \frac{\alpha - 1}{2}\log\left(C^{\frac{1}{\alpha}}z\right) + \cdots. \tag{29}$$

Then the confinement criterion becomes the condition $\alpha \geq 1$. From (8) and (28) we find that the condition $\alpha \geq 1$ implies the existence of a curvature singularity at $z \to \infty$. Interestingly, a WKB analysis of the glueball spectrum [4] leads to the stronger restriction $\alpha = 2$ that corresponds to asymptotically linear Regge trajectories $m_n^2 \sim n$. In this work we take a quadratic dilaton $\Phi(z) = z^2$ in the IR to guarantee confinement and an approximate linear glueball spectrum. The UV, on the other hand, differs significantly from the proposal of [3,4] where instead of imposing asymptotic freedom we consider a CFT deformation, inspired by the work of [6,7]. But first we finish this section by reviewing below how the Schrödinger equations, which determine the glueball spectrum, arise from the linearized dilaton-gravity equations.

[4]This is equivalent to the statement $\partial_u A \leq -1/\ell$, obtained in [4], where u is the domain-wall coordinate related to z by $dz = \zeta du$.

C. Linearized dilaton-gravity equations

The linearized version of the dilaton-gravity equations is obtained by expanding at first order both sides of (15) and (17), with $\Phi \to \Phi + \chi$ and $g_{mn} \to e^{2A}(\eta_{mn} + h_{mn})$, where χ and h_{mn} are first order perturbations in the dilaton and the reference background metric, respectively. The resulting equations take the form

$$R^{(1)}_{mn} = \frac{8}{3}\partial_{(m}\Phi\partial_{n)}\chi - \frac{1}{3}e^{2A}[V h_{mn} + (\partial_\Phi V)\chi\eta_{mn}], \quad (30)$$

$$\frac{4}{3}(\nabla^2\Phi)^{(1)} = -\frac{1}{2}(\partial^2_\Phi V)\chi, \quad (31)$$

where $R^{(1)}_{mn}$ is given by (11),

$$(\nabla^2\Phi)^{(1)} = e^{-2A}\Big\{[\partial_z^2 + 3A'\partial_z + \Box]\chi - \Big[\phi' + \partial_\mu\mathcal{A}^\mu - \frac{1}{2}h' + 2\phi(\partial_z + 3A')\Big]\Phi'\Big\}, \quad (32)$$

and recall that $h_{zz} = 2\phi$, $h_{z\mu} = \mathcal{A}_\mu$ and $h^\mu{}_\mu = h$. Taking the components $(zz, z\mu, \mu\nu)$ of the linearized Einstein equations (30), the system (30) and (31) becomes

$$[\partial_z + A']\Big(\partial_\mu\mathcal{A}^\mu - \frac{1}{2}h'\Big) + 4A'\phi' - \Box\phi - \frac{8}{3}\Phi'\chi' + 2\phi(A'' + 3A'^2) - \frac{8}{9}\chi[\partial_z + 3A']\Phi' = 0, \quad (33)$$

$$\frac{1}{2}\partial_\nu h'^\nu_\mu - \frac{1}{2}\partial_\mu h' + \frac{1}{2}\partial_\nu\mathcal{F}_\mu{}^\nu + 3A'\partial_\mu\phi - \frac{4}{3}\Phi'\partial_\mu\chi = 0, \quad (34)$$

$$[\partial_z + 3A']\partial_{(\mu}\mathcal{A}_{\nu)} - \frac{1}{2}[\partial_z^2 + 3A'\partial_z + \Box]h_{\mu\nu} + \partial_\rho\partial_{(\mu}h^\rho_{\nu)} - \frac{1}{2}\partial_\mu\partial_\nu(2\phi + h) + A'\Big[\phi' + \partial_\rho\mathcal{A}^\rho - \frac{1}{2}h'\Big]\eta_{\mu\nu} + 2(A'' + 3A'^2)\phi\eta_{\mu\nu} - \frac{8}{9}\chi[\partial_z + 3A']\Phi'\eta_{\mu\nu} = 0, \quad (35)$$

$$[\partial_z^2 + 3A'\partial_z + \Box]\chi - \Big[\phi' + \partial_\mu\mathcal{A}^\mu - \frac{1}{2}h' + 2\phi(\partial_z + 3A')\Big]\Phi' + \frac{3}{8}e^{2A}(\partial^2_\Phi V)\chi = 0, \quad (36)$$

where we have used the result (11) for the Ricci tensor and we have also used the following background relations:

$$\frac{1}{3}e^{2A}V = A'' + 3A'^2, \qquad \frac{1}{3}e^{2A}\partial_\Phi V = -\frac{8}{9}[\partial_z + 3A']\Phi'. \quad (37)$$

As explained in [24], the next step is to decompose the four-vector $\mathcal{A}_\mu$ and the symmetric tensor $h_{\mu\nu}$ into irreducible representations of the Lorentz group, i.e.,

$$\mathcal{A}_\mu = \mathcal{A}^T_\mu + \partial_\mu\mathcal{W},$$
$$h_{\mu\nu} = h^{TT}_{\mu\nu} + 2\partial_{(\mu}\mathcal{V}^T_{\nu)} + 2\partial_\mu\partial_\nu\mathcal{E} + 2\psi\eta_{\mu\nu}, \quad (38)$$

where $\mathcal{A}^T_\mu$ and $\mathcal{V}^T_\mu$ are divergenceless vectors, $h^{TT}_{\mu\nu}$ is a traceless and divergenceless tensor and $\mathcal{W}, \mathcal{E}, \psi$ are Lorentz scalars. Applying the decomposition (38) into the dilaton-gravity equations (33)–(36), we find one tensorial equation,

$$[\partial_z^2 + 3A'\partial_z + \Box]h^{TT}_{\mu\nu} = 0, \quad (39)$$

two vectorial equations,

$$[\partial_z + 3A'](\mathcal{A}^T_\mu - \mathcal{V}^{T'}_\mu) = 0, \quad (40)$$

$$\Box(\mathcal{A}^T_\mu - \mathcal{V}^{T'}_\mu) = 0, \quad (41)$$

and five scalar equations,

$$[\partial_z + 3A'](\mathcal{W} - \mathcal{E}') - 2\psi - \phi = 0, \quad (42)$$

$$-[\partial_z^2 + 3A'\partial_z + \Box]\psi + A'[\phi' - 4\psi' + \Box(\mathcal{W} - \mathcal{E}')] + 2\phi(A'' + 3A'^2) - \frac{8}{9}\chi[\partial_z + 3A']\Phi' = 0, \quad (43)$$

$$-3\psi' + 3A'\phi - \frac{4}{3}\Phi'\chi = 0, \quad (44)$$

$$[\partial_z + A'][\Box(\mathcal{W} - \mathcal{E}') - 4\psi'] + 4A'\phi' - \Box\phi - \frac{8}{3}\Phi'\chi' + 2\phi(A'' + 3A'^2) - \frac{8}{9}\chi[\partial_z + 3A']\Phi' = 0, \quad (45)$$

$$[\partial_z^2 + 3A'\partial_z + \Box]\chi - [\phi' + \Box(\mathcal{W} - \mathcal{E}') - 4\psi' + 2\phi(\partial_z + 3A')]\Phi' + \frac{3}{8}e^{2A}(\partial^2_\Phi V)\chi = 0. \quad (46)$$

The tensorial equation (39) leads to the spectrum of spin 2 glueballs. The vectorial equations (40) and (41) do not lead to normalizable modes so we can set $\mathcal{A}^T_\mu = \mathcal{V}^T_\mu = 0$. From the five scalar equations (42)–(46) only one combination decouples from the rest and describes the spectrum of spin 0 glueballs. Below we describe how this equation can be obtained. Subtracting (43) from (45) and using (42), we obtain the equation

$$[\partial_z^2 - A'\partial_z - \Box]\psi - A'\phi' + A'\Box(\mathcal{W} - \mathcal{E}') + \frac{8}{9}\Phi'\chi' = 0. \quad (47)$$

This equation can be combined with (46) to get rid of the term $\Box(\mathcal{W} - \mathcal{E}')$ and to find

$$[\partial_z^2 + 3A'\partial_z - \Box]\psi + \frac{1}{3X}[\partial_z^2 + 3A'\partial_z + \Box]\chi - 2A'\phi' - 2\frac{\phi}{X}[\partial_z + 3A'](A'X) + \frac{8}{3}A'X\chi' + \frac{1}{8X}e^{2A}(\partial_\Phi^2 V)\chi = 0, \tag{48}$$

where X was defined in (24). Using Eq. (44) to replace ϕ in terms of ψ and χ and the background relations (20) and (37), we arrive at the decoupled equation

$$\xi'' + \left(3A' + 2\frac{X'}{X}\right)\xi' + \Box\xi = 0, \tag{49}$$

where the field ξ is defined by

$$\xi = \psi - \frac{\chi}{3X}. \tag{50}$$

The solutions of Eq. (49) lead to the spectrum of spin 0 glueballs.

1. Schrödinger-like equation—scalar sector

It is possible to rewrite Eq. (49) in a Schrödinger-like form. To do so, we define an auxiliary function B_s as

$$B_s = \frac{3}{2}A + \log X. \tag{51}$$

Substituting $\xi = e^{-B_s}\psi_s$ and introducing the Fourier transform ($\Box \to m_s^2$) in Eq. (49), we get

$$-\psi_s'' + V_s\psi_s = m_s^2\psi_s, \tag{52}$$

where the potential is defined as

$$V_s = (B_s')^2 + B_s''. \tag{53}$$

2. Schrödinger-like equation—tensor sector

Following the same procedure as above in the tensor sector we use the auxiliary function

$$B_t = \frac{3}{2}A, \tag{54}$$

to rewrite (39) in the Schrödinger-like form

$$-\psi_t'' + V_t\psi_t = m_t^2\psi_t, \tag{55}$$

where the potential is defined as

$$V_t = (B_t')^2 + B_t''. \tag{56}$$

Interestingly, the difference between the spin 0 and spin 2 sectors lies in the term $B_s - B_t = \log(X)$. This is an important feature when calculating the glueball spectrum that explains the nondegeneracy of scalar and tensor glueballs.

III. EFFECTIVE HOLOGRAPHIC QCD

As anticipated in the previous sections, our work explores the idea of a massive term for the dilaton in the UV as the dual of a CFT deformation $\delta\mathcal{L} = \phi_0\mathcal{O}$. The coupling ϕ_0 and the operator $\mathcal{O}$ have conformal dimensions ϵ and $4-\epsilon$, respectively. The latter is related to the QCD operator $\mathrm{Tr}F^2$. The idea of a CFT relevant deformation was proposed in [6,7] when constructing a holographic model for QCD at finite temperature. Since the CFT deformation takes place at a particular energy scale μ^*, which becomes an upper energy bound for the four-dimensional theory, we dub this approach effective holographic QCD.

In this work we show that this type of UV asymptotics, at zero temperature, is compatible with (explicit) conformal symmetry breaking, confinement, and the glueball spectrum. To achieve this we also constrain the IR in the way proposed in [3,4], namely by considering a quadratic dilaton. Below we describe in more detail the universal UV and IR asymptotic behavior for the family of HQCD backgrounds considered in this work. We also describe specific models that interpolate smoothly between the UV and IR asymptotics. Then in the next section we calculate the glueball spectrum and investigate how the model parameters evolve with the conformal dimension ϵ.

A. CFT deformation in the UV

In the pioneer work [2], Csaki and Reece identified a dynamical dilaton as the five-dimensional scalar field dual to the operator $\mathrm{Tr}F^2$. They initially considered a massless dilaton and obtained a nonzero gluon condensate. However, as found in [2], a massless dilaton leads to a Nambu-Goldstone boson in the spectrum of scalar glueballs, indicating that conformal symmetry was spontaneously broken. It is important to remark, however, that the background of [2] requires additional boundary conditions at the singularity, which brings some ambiguities [4]. As a mechanism for explicit conformal symmetry breaking, the authors of [2] proposed the holographic implementation of asymptotic freedom in the UV. This was correctly implemented in the IHQCD background developed by Gursoy *et al.* [3,4]. The background of [3,4] is also consistent with linear confinement in the IR and does not require additional boundary conditions at the singularity.

As explained above, instead of implementing asymptotic freedom in the UV, we are interested in explicitly breaking conformal invariance through a UV mass term for the dilaton. According to the AdS/CFT dictionary, the mass M of a five-dimensional dilaton, responsible for deforming AdS space, is related to the conformal dimension Δ of a dual scalar operator $\mathcal{O}$, responsible for deforming the

four-dimensional CFT, by the equation $M^2\ell^2 = \Delta(\Delta-4)$. Then by considering a relevant operator with dimension $\Delta = 4-\epsilon$, we end up with a nonzero mass for the dilaton. We later relate this operator to the QCD operator $\mathrm{Tr}F^2$ and investigate the connection between the trace anomaly of deformed CFTs and the QCD trace anomaly. This in turn sheds some light on the role played by the conformal dimension ϵ in effective holographic QCD.

Let us first consider an expansion of the dilaton potential around the UV minimum $\Phi = 0$, which includes a constant term, associated with a negative cosmological constant, and a nonzero mass term,

$$V(\Phi) = \frac{12}{\ell^2} - \frac{4}{3}M^2\Phi^2 + \cdots, \tag{57}$$

where the ellipses denote higher powers of Φ. On the basis of Eqs. (19), one finds that the constant term in (57) leads to the AdS asymptotics whereas the mass term implies the following near-boundary behavior for the dilaton,

$$\Phi = \phi_0 z^{\Delta_-} + G z^{\Delta_+} + \cdots, \tag{58}$$

where $\Delta_+ = \Delta = 4-\epsilon$ and $\Delta_- = 4-\Delta_+ = \epsilon$, both related to the five-dimensional mass by $M^2\ell^2 = -\Delta_+\Delta_-$. Following the AdS/CFT dictionary, we interpret the coefficient ϕ_0 as the source for the dual operator $\mathcal{O}$. The coefficient G is related to the VEV of $\mathcal{O}$. We also remind the reader that the CFT deformation $\delta\mathcal{L} = \phi_0\mathcal{O}$ takes place at some cutoff energy μ^*.

Considering the perturbative expansion for Φ, given by (58), we find from Eq. (22) the asymptotic expansions for $\zeta(z)$ and the warp factor $A(z) = -\log\zeta(z)$,

$$\begin{aligned}\zeta(z) &= \frac{z}{\ell}\left[1 + \frac{2\Delta_-}{9(1+2\Delta_-)}\phi_0^2 z^{2\Delta_-} + \frac{2\Delta_-\Delta_+}{45}\phi_0 G z^4 \right.\\ &\left. + \frac{2\Delta_+}{9(1+2\Delta_+)}G^2 z^{2\Delta_+} + \cdots\right],\\ A(z) &= -\log(z/\ell) - \frac{2\Delta_-}{9(1+2\Delta_-)}\phi_0^2 z^{2\Delta_-} - \frac{2\Delta_-\Delta_+}{45}\phi_0 G z^4\\ &- \frac{2\Delta_+}{9(1+2\Delta_+)}G^2 z^{2\Delta_+} - \cdots.\end{aligned} \tag{59}$$

If instead of a mass term for the dilaton, we followed the prescription of [3,4] and imposed asymptotic freedom, we would obtain a UV asymptotics involving logarithmic terms to be consistent with the logarithmic dependence of the 't Hooft coupling with the energy.

Since we know the asymptotic behavior of the warp factor (59) we are also able to find, from the second equation in (23), the small z behavior of the superpotential,

$$\ell W(z) = \frac{9}{4} + \frac{\Delta_-}{2}\phi_0^2 z^{2\Delta_-} + \frac{\Delta_-\Delta_+}{2}\phi_0 G z^4 + \frac{\Delta_+}{2}G^2 z^{2\Delta_+} + \cdots. \tag{60}$$

Alternatively, we can solve the differential Eq. (23) for the superpotential $W(\Phi)$ for a dilaton potential $V(\Phi)$ given by (57) and find [16,17]

$$\ell W_\pm(\Phi) = \frac{9}{4} + \frac{\Delta_\pm}{2}\Phi^2 + \cdots, \tag{61}$$

which is in agreement with Eq. (60). From the above results it is easy to find the asymptotic expansion for the field $X(z)$, defined in (24). The expansion takes the form

$$3X(z) = -\Delta_-\phi_0 z^{\Delta_-} - \Delta_+ G z^{\Delta_+} + \cdots. \tag{62}$$

The results above also tell us how the metric behaves near the boundary,

$$\begin{aligned}ds^2 = \frac{\ell^2}{z^2}&\left(1 - \frac{4\Delta_-}{9(1+2\Delta_-)}\phi_0^2 z^{2\Delta_-} - \frac{4\Delta_-\Delta_+}{45}\phi_0 G z^4 - \cdots\right)\\ &\times [dz^2 + \eta_{\mu\nu}dx^\mu dx^\nu].\end{aligned} \tag{63}$$

We finish this subsection writing the asymptotic expansion of the dilaton (58) in a form that is useful when implementing the numerical procedure,

$$\Phi(z) = \hat{\phi}_0(\Lambda z)^\epsilon + (\Lambda z)^{4-\epsilon} + \cdots, \tag{64}$$

where the parameters $\hat{\phi}_0$ and Λ are related to ϕ_0 and G by

$$\phi_0 = \hat{\phi}_0\Lambda^\epsilon, \qquad G = \Lambda^{4-\epsilon}. \tag{65}$$

The parameter Λ has conformal dimension 1 and plays a role similar to Λ_{QCD} whereas the parameter $\hat{\phi}_0$ is the dimensionless version of the coupling ϕ_0. For all practical purposes $\hat{\phi}_0$, Λ and ϵ are the relevant parameters of the model. We see later that, for fixed ϵ, the parameters $\hat{\phi}_0$ and Λ can be fit in order to reproduce the glueball spectrum.

B. Confinement in the IR

In Ref. [4], Gursoy *et al.* did a careful analysis that is universal for holographic QCD backgrounds arising from a dilaton-gravity theory. Specifically, considering the general confinement criterion of [22] and also a WKB analysis for the glueball spectrum, they found that a quadratic dilaton in the IR guarantees confinement and an approximate linear spectrum for glueballs. Remarkably, this quadratic dilaton had been already proposed in the phenomenological soft-wall model [5], in order to arrive at a linear spectrum for mesons. Interestingly, a quadratic dilaton in the IR also

provides the T^2 correction to the stress tensor trace anomaly of a deconfined plasma [25].

Motivated by the results of [4], we consider in this work the following dilaton asymptotic behavior at large z:

$$\Phi(z) = Cz^2 + \cdots, \tag{66}$$

where the dots indicate terms that depend on negative powers of z. Using the IR asymptotic relation (28) between $A(z)$ and $\Phi(z)$, we construct the asymptotic forms for the warp factor $A(z)$ and the function $\zeta(z)$,

$$\begin{aligned} A(z) &= -\frac{2}{3}Cz^2 + \frac{1}{2}\log(\sqrt{C}z) + \cdots, \\ \zeta(z) &= (\sqrt{C}z)^{-1/2}\exp\left(\frac{2}{3}Cz^2\right) + \cdots. \end{aligned} \tag{67}$$

With this information at hand, we use the second equation in (23) to write down the superpotential,

$$W(z) = 3C^{\frac{3}{4}}\sqrt{z}\exp\left(\frac{2}{3}Cz^2\right) + \cdots. \tag{68}$$

We get the asymptotic expansion of X using Eqs. (66) and (67) and the definition (24),

$$X = -\frac{1}{2}\left[1 + \frac{3}{8Cz^2} + \cdots\right] = -\frac{1}{2}\left[1 + \frac{3}{8}\frac{1}{\Phi} + \cdots\right]. \tag{69}$$

Substituting this expression for $X(\Phi)$ in (24) and integrating the resulting equation in Φ, we obtain the asymptotic behavior for the superpotential in terms of Φ,

$$W(\Phi) \propto \Phi^{1/4}\exp\left(\frac{2}{3}\Phi\right) + \cdots, \tag{70}$$

which is consistent with (68). Similarly, the asymptotic expression for the dilaton potential in the radial coordinate z can be found from Eqs. (20) and (67),

$$\begin{aligned} V(z) &= 16C^{\frac{3}{2}}z\exp\left(\frac{4}{3}Cz^2\right) + \cdots, \\ \frac{V'(z)}{V(z)} &= \frac{8}{3}Cz + \frac{1}{z} + \cdots. \end{aligned} \tag{71}$$

For completeness, we write down the dilaton potential as a function of Φ. Substituting Eq. (70) into the differential Eq. (23) and taking the leading term, we get

$$\begin{aligned} V(\Phi) &\propto \Phi^{1/2}\exp\left(\frac{4}{3}\Phi\right) + \cdots, \\ \frac{\partial_\Phi V(\Phi)}{V(\Phi)} &= \frac{4}{3} + \frac{1}{2\Phi} + \cdots. \end{aligned} \tag{72}$$

The results (68) and (71) satisfy the general criteria presented in [3,4] to guarantee linear confinement in the IR. It is interesting to point out the difference between this IR asymptotics and the one considered in [6,7]. In that case the ratio $\partial_\Phi V(\Phi)/V(\Phi)$ is a constant because the potential goes like $\exp(\gamma\Phi)$, where γ is a constant. Here we have considered the IR asymptotics of [3,4], where the ratio $\partial_\Phi V(\Phi)/V(\Phi)$ has a subleading term that decreases as $1/z^2$ because the dilaton is quadratic in the IR.

From the result (67), we see that the metric shrinks to 0 at large z as

$$ds^2 = \sqrt{C}z\exp\left(-\frac{4}{3}Cz^2 + \cdots\right)[dz^2 + \eta_{\mu\nu}dx^\mu dx^\nu]. \tag{73}$$

As explained above, this leads to a curvature singularity at $z \to \infty$, i.e. a divergent Ricci scalar.

The above results were obtained in the Einstein frame, where the warp factor decreases monotonically. If we calculated the warp factor in the string frame, $A_s(z)$, we would see that it has a minimum, associated with the fundamental string tension [4].

Again, we write the IR dilaton asymptotics (66) in a convenient form,

$$\Phi(z) = (\Lambda z)^2 + \cdots. \tag{74}$$

Note that we are using the same coefficient Λ that appeared already in the UV expansion. This implies a relation between the IR coefficient C at large z and the UV coefficient G at small z. In the next section, we show that the parameter Λ is responsible for fixing the scale of the glueball masses when comparing the numerical results against lattice data.

C. UV/IR interpolation

In the pioneer soft-wall model [5], a quadratic dilaton was introduced by hand to get the desired behavior in the dual QCD-like theory, namely, the Regge-like behavior $m^2 \propto n$. As explained before, starting from [2] there have been interesting proposals for holographic QCD considering a dilaton field dynamically coupled to the metric. This in turn leads to a nonzero gluon condensate and confinement. A particularly interesting proposal was considered recently in [26,27] where an analytic function was used to interpolate the dilaton between a quartic form in the UV and a quadratic form in the IR. However, as explained before, a quartic dilaton in the UV necessarily leads to an unacceptable massless mode in the scalar sector of glueballs [2].[5]

In Sec. II C we described the process of linearizing the dilaton-gravity equations to arrive at the equations

[5]This result is missing in Ref. [26,27] because the authors did not describe scalar glueballs in terms of scalar perturbations in dilaton gravity.

governing the dynamics of the scalar and tensor glueballs. A careful analysis of these equations suggests two possible solutions for the massless mode problem. The first solution, originally proposed in [2] and beautifully realized in [3,4], consists of introducing asymptotic freedom in the UV. However, the price to be paid when introducing asymptotic freedom is the presence of logarithmic corrections in the warp factor and the dilaton which make the AdS/CFT dictionary more involved [28,29]. The second solution, considered in this work, is implementing a CFT deformation of the form $\delta\mathcal{L} = \phi_0\mathcal{O}$, $\mathcal{O}$ being a relevant operator dual to the dilaton. The conformal dimension of $\mathcal{O}$ was set to $\Delta = 4 - \epsilon$ in Eq. (58), with ϵ being small. Mapping this operator to the QCD operator $\mathrm{Tr}F^2$ signalizes the presence of a UV cutoff μ^* in the QCD-like theory, as advocated in [6,7].

The UV asymptotics corresponding to the CFT deformation was described in Sec. III A whereas the IR asymptotics leading to linear confinement was described in Sec. III B. In particular, the UV and IR asymptotics for the dilaton were given in (64) and (74) respectively. There are two immediate options for interpolating between the UV and IR asymptotics. We can define an analytic function for the dilaton that interpolates from the UV to the IR and solve numerically for the warp factor and the potential $V(z)$. The models arising in this approach are called models A. The second possibility is to interpolate the warp factor between the two regimes, so that we get numerically the dilaton and the potential $V(z)$. The models in this second approach are called models B. In the following we present and analyze the first case (models A) and leave the analysis of models B for Appendix B.

In Sec. IV we show how these effective holographic QCD models (models A and B) lead to a realistic spectrum for scalar and tensor glueballs. In Sec. V we take advantage of the fact that the effective holographic QCD approach allows the use of the standard AdS/CFT dictionary and calculate the VEV of the operator $\mathcal{O}$. We relate this VEV to the gluon condensate $\langle \mathrm{Tr}F^2 \rangle$ and discuss the trace anomaly of deformed CFTs in connection with the QCD scale anomaly. A general discussion of the massless mode and its resolution is made in Appendix A.

1. Models A: Analytic form for the dilaton field

As explained above, in models A we interpolate the dilaton field, from the UV asymptotics (64) to the IR asymptotics (74), in order to describe a CFT deformation in the UV and confinement in the IR. Among the many possibilities for interpolating the dilaton between the UV and IR asymptotics, we choose two of them.

The first interpolation (model A1) is constructed in terms of powers of the holographic coordinate,

$$\Phi(z) = \hat{\phi}_0(\Lambda z)^\epsilon + \frac{(\Lambda z)^{4-\epsilon}}{1 + (\Lambda z)^{2-\epsilon}}, \tag{75}$$

where the parameters $\hat{\phi}_0$, Λ, and ϵ were already defined below Eq. (64). This is the simplest way of interpolating from the UV to the IR.

The second interpolation (model A2) introduces a hyperbolic tangent function,

$$\Phi(z) = \hat{\phi}_0(\Lambda z)^\epsilon + (\Lambda z)^2 \tanh\left[(\Lambda z)^{2-\epsilon}\right]. \tag{76}$$

It is easy to see that both equations (75) and (76) recover the previous asymptotic expansions in the UV and IR, Eqs. (64) and (74), respectively. The warp factor, on the other hand, is obtained by solving the first differential equation in (20).

As explained previously, the dilaton field $\Phi(z)$ and warp factor $A(z)$ depend only on the parameters $\hat{\phi}_0$, Λ and ϵ. The parameter Λ is used to fix the energy scale while the value of $\hat{\phi}_0$ plays the role of a dimensionless coupling. Our numerical strategy is to fix the conformal dimension ϵ and fit the parameters $\hat{\phi}_0$ and Λ using the masses of the first two scalar glueballs (taken from lattice QCD). This analysis is developed in Sec. IV.

2. Numerical analysis of the background

Having specified the models A, where the dilaton is an analytic function, we can solve numerically the dilaton-gravity equations (20), with the appropriate boundary conditions, and explore the evolution of the geometric quantities such as the warp factor $A(z)$, the field $X(z)$ and the superpotential $W(z)$. The parameters that we use to get the results and plot the figures in this section are presented in Table I and are justified in Sec. IV D. Our goal here is to show the nonsingular behavior of these quantities. The dilaton field $\Phi(z)$, dual to the relevant operator $\mathcal{O}$, is shown in Fig. 1. The effect of the conformal dimension ϵ is evident near the boundary where the dilaton field goes as $\sim\phi_0 z^\epsilon$ (see the box in the figure), with $\phi_0 = \hat{\phi}_0\Lambda^\epsilon$. This is the dominant term responsible for the explicit breaking of conformal invariance. Figure 1 also shows the asymptotic behavior of the dilaton $\sim\Lambda^2 z^2$ in the IR, responsible for

TABLE I. The values of the parameters for models A1 and A2 used to get the results presented in Sec. III C 2 for $\epsilon = 0.1$.

Models	$\hat{\phi}_0$	Λ(MeV)	ϕ_0(MeV$^\epsilon$)	$G(10^{11}$ MeV$^{4-\epsilon})$	$C(10^5$ MeV$^2)$
Model A1	5.59	742.75	10.83	1.57	5.52
Model A2	5.33	677.98	10.23	1.10	4.60

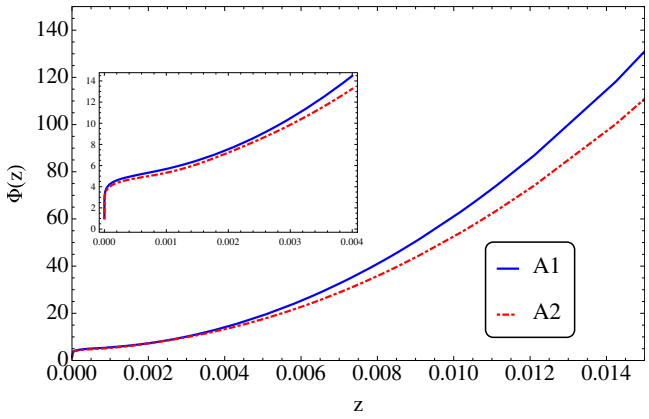

FIG. 1. Dilaton profiles for models A1 and A2, defined in (75) and (76) respectively, for $\epsilon = 0.1$ and the parameters given in Table I.

confinement and a linear spectrum. The difference between models A1 and A2 lies in the values of the parameters $\hat{\phi}_0$ and Λ, in addition to the interpolation form.

On the left panel of Fig. 2, we plot the numerical solution for the Einstein-frame warp factor $A(z)$ in models A1 and A2. These results are consistent with the UV and IR asymptotics, given by Eqs. (59) and (67), respectively. The difference between models A1 and A2 lies in the region for large z. As we see in Sec. IV, the effect of this difference is realized in the glueball spectrum. The right panel in Fig. 2 shows the string-frame warp factor $A_s(z)$, obtained from Eq. (26). This function has a minimum at some $z = z^*$, which is consistent with the confinement criterion described in Sec. II B.

Another important geometric quantity is the field $X(z)$, defined in Eq. (24). As shown on the left panel in Fig. 3, this quantity has the same asymptotic behavior for both models A1 and A2, and the relevant difference lies in the intermediate region. The presence of confinement in the IR is consistent with $X(z)$ approaching a constant value for large z. As discussed in [15,16], the field X can be interpreted as a bulk effective β-function associated with the four-dimensional RG flow driven by the operator $\mathcal{O}$.

The breaking of conformal invariance can be appreciated by looking at the superpotential $W(z)$, obtained from the second equation in (23). As a consequence of the CFT deformation in the UV, the superpotential raises rapidly with the coordinate z, as shown on the right panel in Fig. 3. This behavior was previously noticed for the case of nearly marginal operators [15]. In contrast with $X(z)$, the difference in $W(z)$ between models A1 and A2 lies in the IR. Those differences play a role in the spectrum of glueballs, which are calculated in Sec. IV.

D. The vacuum energy density

A very important quantity in holographic QCD is the vacuum energy density $\langle T^{00}\rangle$. In the absence of a CFT deformation, we expect $\langle T^{00}\rangle$ to vanish since the four-dimensional theory lives in Minkowski spacetime.[6] In our case, the CFT deformation $\delta\mathcal{L} = \phi_0\mathcal{O}$ generates a nontrivial negative $\langle T^{00}\rangle$ that is interpreted as the QCD vacuum energy density.

In holography the vacuum energy of a four-dimensional theory corresponds to the on-shell Euclidean action associated with the five-dimensional gravitational background. In dilaton gravity the action is given by

$$S = S_E + S_{GH}, \tag{77}$$

where

$$S_E = -M_p^3 N_c^2 \int d^4x \times \int_{z_0}^{\infty} dz\sqrt{g}\left(R - \frac{4}{3}g^{mn}\partial_m\Phi\partial_n\Phi + V(\Phi)\right), \tag{78}$$

and

$$S_{GH} = M_p^3 N_c^2 \int d^4x\sqrt{\gamma}2K|_{z=z_0} \tag{79}$$

is the Gibbons-Hawking boundary term. In holographic renormalization one first defines the boundary at $z = z_0$ and takes the limit $z_0 \to 0$ only at the very end of the renormalization process. We have introduced in (79) the induced metric $\gamma_{\mu\nu} = \exp(2A)\eta_{\mu\nu}$ and the trace of the extrinsic curvature K, given by

$$K = \nabla_m\eta^m, \qquad \eta^m = \zeta(z)\delta_z^m, \tag{80}$$

where $\zeta(z)$ is defined in (21). As shown in [4], using the equations of motion (19) the on-shell (o-s) action densities take the form

$$\mathcal{S}_E^{\text{o-s}} = \frac{S_E^{\text{o-s}}}{V_4} = -2M_p^3 N_c^2 e^{3A(z_0)}A'(z_0),$$
$$\mathcal{S}_{GH}^{\text{o-s}} = \frac{S_{GH}^{\text{o-s}}}{V_4} = 8M_p^3 N_c^2 e^{3A(z_0)}A'(z_0), \tag{81}$$

where V_4 is the four-dimensional volume. Thus we find the bare energy density

$$\langle T^{00}\rangle = \mathcal{S}_E^{\text{o-s}} + \mathcal{S}_{GH}^{\text{o-s}} = 6M_p^3 N_c^2 e^{3A(z_0)}A'(z_0). \tag{82}$$

The near-boundary asymptotic behavior of the warp factor $A(z)$ was obtained in (59). Using that result in (82) one finds terms that diverge when z_0 goes to 0. We consider a minimal subtraction (MS) scheme where the divergent

[6]When the four-dimensional CFT lives in a curved background one usually gets a nonvanishing vacuum energy density.

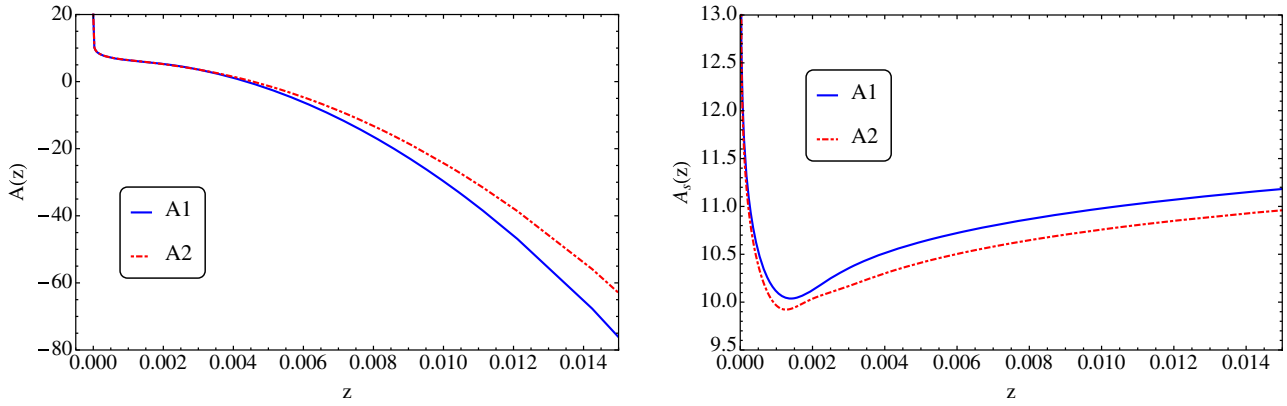

FIG. 2. Left panel: The Einstein-frame warp factor $A(z)$ for models A1 and A2, obtained by solving numerically the dilaton-gravity equations (20). Right panel: The string-frame warp factor $A_s(z)$ for models A1 and A2, obtained from Eq. (26). The results shown in this figure correspond to $\epsilon = 0.1$ and the parameters given in Table I.

terms are eliminated by adding the appropriate counterterms. After this renormalization process one finally takes the limit $z_0 \to 0$. Most of the nondivergent terms vanish in this limit and the surviving finite piece becomes the renormalized vacuum energy density,

$$\mathcal{E}^{ren}_{\rm QCD} = \langle T^{00}\rangle^{ren} = -\frac{4}{15}(M_p\ell)^3 N_c^2 \epsilon(4-\epsilon)\phi_0 G, \quad (83)$$

where the superscript *ren* means renormalized. The numerical results for this renormalized vacuum energy density are shown in the next section. Here we just notice that the vacuum energy density is negative and therefore lower than the (zero) energy of the CFT vacuum. We remark, however, that the result (83) may change if we use a different renormalization scheme. Note also from (65) that $\phi_0 G = \hat{\phi}_0 \Lambda^4$ has conformal dimension 4, which is indeed the protected conformal dimension of $T^{\mu\nu}$.

IV. GLUEBALL SPECTRUM

Glueballs are bound states of gluons predicted by QCD. So far, they have not been detected although there is a recent claim that the $f_0(1710)$ scalar particle may actually be the scalar glueball state 0^{++} [30,31]. Furthermore, it was also recently proposed that the odd glueball (oddball) 0^{--} could be detected soon by the experiments BESIII, BELLEII, Super-B, PANDA, and LHCb [32], although there is some controversy on this prediction [33]. Other interesting glueball states, as for example, 2^{++}, 0^{-+} and 1^{--} are under investigation and have candidates in the particle spectrum [34].

In this work, we are particularly interested in the scalar 0^{++} and tensor 2^{++} glueball states, as well as their radial excitations. The investigation of those glueball states has been made in lattice QCD and other nonperturbative approaches. For a review, see for instance [34]. Previous holographic approaches to the glueball spectrum include the Witten's model [35–37], the Klebanov-Strassler model

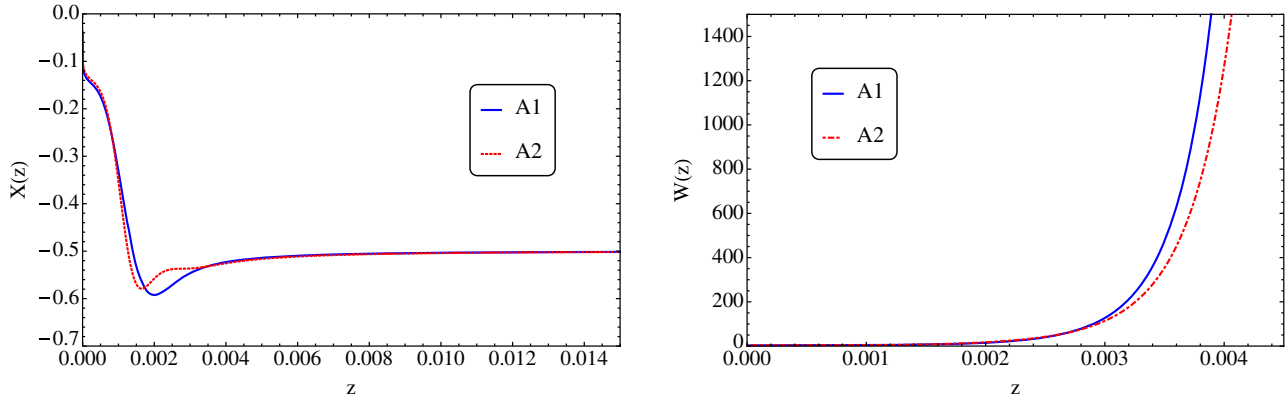

FIG. 3. Left panel: The field $X(z)$ for models A1 and A2, obtained from Eq. (24). Right panel: The superpotential $W(z)$ for models A1 and A2, obtained from the second equation in (23). The results shown in this figure correspond to $\epsilon = 0.1$ and the parameters given in Table I.

[38–40], the Maldacena-Nunez model [41,42], the hardwall model [43–45], the soft-wall model [46] and extensions [47,48], dynamical soft-wall models [26,27,49,50] and IHQCD models [4].

We find the spectrum of scalar 0^{++} and tensor 2^{++} glueball states from solving the differential equations (52) and (55), respectively. In those Schrödinger-like equations the glueball states are represented by wave functions ψ_s and ψ_t. Under suitable boundary (asymptotic) conditions on these wave functions, the mass spectrum of the respective sector is found. As explained in the previous section, the parameters in our models are $\hat{\phi}_0$, Λ and ϵ and the strategy is the following: for each value of ϵ the parameters $\hat{\phi}_0$ and Λ are fixed using as input the lattice QCD results for the first two scalar glueballs [51]. At the end of the numerical calculation, we compare our results for all the other glueball states against lattice QCD data [51], and the results obtained in the IHQCD model [4].

In the numerical calculation it is convenient to rewrite the interpolations (75) and (76) in terms of a dimensionless coordinate $u = \Lambda z$,

$$\Phi(z) = \hat{\phi}_0 u^{\epsilon} + \frac{u^{4-\epsilon}}{1+u^{2-\epsilon}}, \tag{84}$$

$$\Phi(u) = \hat{\phi}_0 u^{\epsilon} + u^2 \tanh(u^{2-\epsilon}). \tag{85}$$

Notice that the parameter Λ has disappeared in (84) and (85). This is because the u coordinate is dimensionless and the Schrödinger-like equation in this coordinate leads to a spectrum where the masses are given in units of Λ. We remind the reader that fixing Λ fixes also the VEV coefficient $G = \Lambda^{4-\epsilon}$ in the UV as well as the IR coefficient $C = \Lambda^2$ characterizing confinement.

A. Analysis of the effective potentials

The spectrum of glueballs depends on the form of the effective potentials V_s and V_t, which appear in the Schrödinger-like equations (52) and (55). Here we present an analysis of those potentials.

Let us start with the effective potential V_s for the scalar sector, defined in Eq. (53). In terms of the dimensionless variable u, this potential takes the form

$$\frac{V_s(u)}{\Lambda^2} = [\partial_u B_s(u)]^2 + \partial_u^2 B_s(u), \tag{86}$$

with

$$B_s(u) = \frac{3}{2}A(u) + \log[X(u)]. \tag{87}$$

From Eqs. (59) and (62), we know how $A(u)$ and $X(u)$ behave in the UV. Using those results we get the UV asymptotic behavior of $B_s(u)$,

$$B_s(u) = \left(-\frac{3}{2}+\epsilon\right)\log u + \cdots. \tag{88}$$

Our hypothesis is that the conformal dimension ϵ is small. Then the leading term of the scalar potential (86) takes the form

$$\frac{V_s(u)}{\Lambda^2} = \left(\frac{15}{4} + M^2\ell^2\right)\frac{1}{u^2}, \tag{89}$$

where we have introduced the dilaton mass term $M^2\ell^2 = \epsilon(\epsilon-4)$. This term is responsible in the UV for the explicit break of conformal symmetry.

Now we turn attention to the effective potential V_t for the tensor sector, defined in Eq. (56). In terms of the u coordinate it takes the form

$$\frac{V_t(u)}{\Lambda^2} = [\partial_u B_t(u)]^2 + \partial_u^2 B_t(u), \tag{90}$$

with

$$B_t(u) = \frac{3}{2}A(u). \tag{91}$$

The UV asymptotic behavior of this potential is obtained from the asymptotic behavior of $A(u)$, given by Eq. (59). The result is simply

$$\frac{V_t(u)}{\Lambda^2} = \frac{15}{4u^2}. \tag{92}$$

Notice that the conformal dimension ϵ does not affect the UV asymptotic behavior of the tensor potential.

In the IR regime, at large u, the asymptotic behavior for $A(u)$ and $X(u)$ is given by Eqs. (67) and (69) respectively. Then the functions $B_{s,t}(u)$ have the IR asymptotic form

$$B_{s,t}(u) = -u^2 + \cdots. \tag{93}$$

Therefore, the IR asymptotic behavior of the effective potentials (for both sectors) takes the form

$$\frac{V_{s,t}(u)}{\Lambda^2} = 4u^2. \tag{94}$$

In Fig. 4 we show the effective potentials, obtained numerically, for models A1 and A2 at $\epsilon = 0.01$ and $\hat{\phi}_0 = 50$. The plots are consistent with the asymptotic results (89), (92) and (94). As expected, the difference between models A1 and A2 lies in the intermediate region.

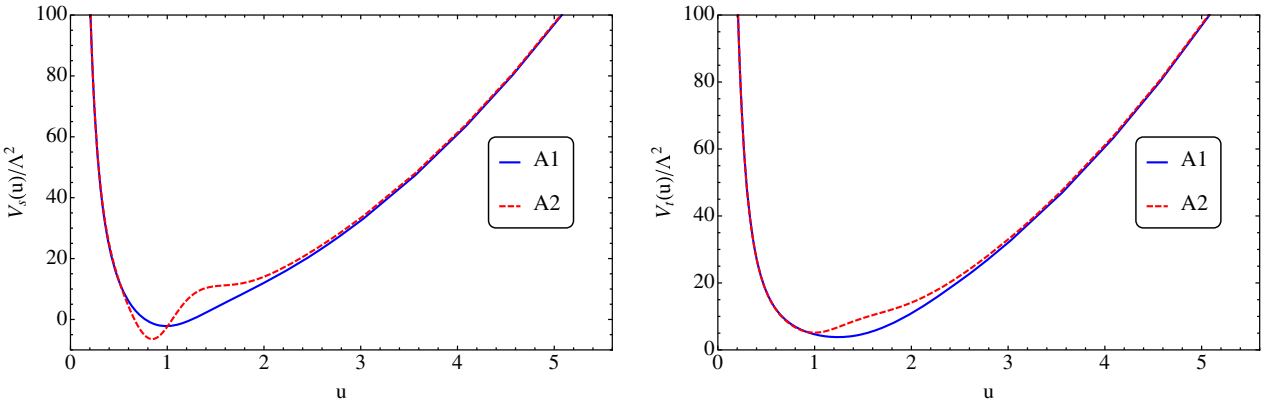

FIG. 4. The scalar (left panel) and tensor (right panel) effective potentials for models A1 and A2 at $\epsilon = 0.01$, $\hat{\phi}_0 = 50$. An analogous figure for models B is shown in Appendix B.

B. UV and IR asymptotic solutions for the wave functions

In this section we find the UV and IR asymptotic solutions for the wave functions ψ_s and ψ_t in the Schrödinger-like equations (52) and (55).

First we look for the UV asymptotic solution for the wave function ψ_s of the scalar sector. Substituting the UV asymptotic form (89) of the potential V_s in the differential Eq. (52), we find

$$-\psi_s''(u) + \left(\frac{3}{2} - \epsilon\right)\left(\frac{5}{2} - \epsilon\right)\frac{1}{u^2}\psi_s(u) = \hat{m}_s^2\psi_s(u), \tag{95}$$

where $\hat{m}_s = m_s/\Lambda$ parametrizes the four-dimensional masses of scalar glueballs in units of Λ. Near the boundary the wave function ψ_s behaves as a power law, $\psi_s(u) = u^{\alpha_1}$. Substituting this ansatz into the differential Eq. (95), and solving the resulting indicial equation, we find two solutions for α_1, namely, $\alpha_1^- = -\epsilon + 5/2$ and $\alpha_1^+ = \epsilon - 3/2$, which means that the asymptotic general solution is of the form

$$\psi_s(u) = c_1 u^{-\epsilon+\frac{5}{2}} + c_2 u^{\epsilon-\frac{3}{2}}. \tag{96}$$

The coefficient c_2 is set to 0 because we are looking for a normalizable solution.

We perform a similar analysis to obtain the UV asymptotic behavior of the wave function ψ_t of the tensor sector. Using the UV asymptotic form of the potential (92), the differential Eq. (55) becomes

$$-\psi_t''(u) + \frac{15}{4u^2}\psi_t(u) = \hat{m}_t^2\psi_t(u), \tag{97}$$

where $\hat{m}_t = m_t/\Lambda$ parametrizes the masses of tensor glueballs in units of Λ. Again, we select the normalizable solution

$$\psi_t(u) = c_3 u^{5/2}. \tag{98}$$

Finally we look for the IR asymptotic behavior of ψ_s and ψ_t. As shown in Eq. (94), the effective potentials of the scalar and tensor sectors have the same asymptotic behavior in the IR. Then both Schrödinger-like equations assume the form

$$-\psi_{s,t}''(u) + 4u^2\psi_{s,t}(u) = \hat{m}_{s,t}^2\psi_{s,t}(u). \tag{99}$$

Solving this equation, we find the IR asymptotic solutions that converge at infinity can be written as

$$\psi_{s,t}(u) = c_4 u^{(\hat{m}_{s,t}^2-2)/4} e^{-u^2}. \tag{100}$$

C. Glueball spectrum at fixed ϵ

The task now is to solve the eigenvalue problem for the differential equations (52) and (55). We solve this problem numerically using a shooting method, which was implemented in a *Mathematica* code.

In order to find a unique solution to a second order differential equation, we need two boundary conditions. There are two typical ways of doing this. We can use the asymptotic UV solutions (96) and (98) and its derivatives, respectively for the scalar and tensor sectors, as boundary conditions at some $u = u_{\min}$, with $u_{\min}$ being very small. Then, we integrate numerically from small u to large u and require that the wave function at large u should behave as in (100). Using those conditions and fixing the parameters ϵ and $\hat{\phi}_0$, we get a discrete spectrum (in units of Λ). Alternatively, we may take the asymptotic IR solutions (100) and their derivatives as initial conditions at some $u = u_{\max}$, with $u_{\max}$ being very large, and integrate numerically from large u to small u requiring the numerical solutions for ψ_s and ψ_t at small u to behave as (96) and (98), respectively.

The numerical results presented in this section were obtained using the first procedure described above. Here we

present our results for models A (introduced in the previous section) as well as for models B1 and B2 (introduced in Appendix B).

In this subsection we present the results for the glueball spectrum at a fixed value of the conformal dimension, namely $\epsilon = 0.01$. At fixed ϵ the parameter $\hat{\phi}_0$ can be fixed by using as input the ratio between the first two scalar glueballs

$$R_{00} = \frac{m_{0^{++*}}}{m_{0^{++}}} = \frac{\hat{m}_{s,1}}{\hat{m}_{s,0}}, \tag{101}$$

where $\hat{m}_{s,0}$ and $\hat{m}_{s,1}$ represent the first two scalar masses and $m_{0^{++}}$ and $m_{0^{++*}}$ are extracted from lattice QCD data [51]. Once $\hat{\phi}_0$ is determined from the ratio R_{00}, we also fix the parameter Λ by comparing the first scalar mass $m_{s,0} = \Lambda \hat{m}_{s,0}$ with the first glueball state $m_{0^{++}}$, extracted from lattice QCD data [51]. Below we describe the results for the glueball spectrum obtained for each one of models A and B.

1. Models A

Implementing the procedure described above for model A1, where the dilaton is given by Eq. (75), we find for $\epsilon = 0.01$ that $\hat{\phi}_0 = 53.62$ and $\Lambda = 737$ MeV. Any other parameter is defined in terms of ϵ, $\hat{\phi}_0$ and Λ and most of them are shown in Table II.

The results for the spectrum of scalar and tensor glueballs in model A1 are shown in the second column of Table III. These results are in good agreement with the lattice QCD calculations [51], and also with the IHQCD model [4]. The largest difference between our results and lattice QCD data is about 4.2% in the case of $m_{0^{++**}}$. We remind the reader that the first two masses in Table III, $m_{0^{++}}$ and $m_{0^{++*}}$, were used to fix $\hat{\phi}_0$ and Λ. Therefore, the predictions of the present models are the ones displayed from the third state (0^{++**}) and below in that table.

The numerical results for the glueball spectrum are well fitted by linear trajectories. For the scalar sector we find the linear trajectory

$$m_{s,n}^2 = \Lambda^2(8.65n + 4.85), \qquad n = 0, 1, 2, \ldots, \tag{102}$$

while for the tensor sector we obtain

TABLE II. The values of the parameters we use to get the spectrum for the glueballs with $\epsilon = 0.01$.

Model	$\hat{\phi}_0$	Λ(MeV)	ϕ_0(MeV$^\epsilon$)	G(MeV$^{4-\epsilon}$)	C(MeV^2)
A1	53.79	736	57.46	2.75×10^{11}	5.42×10^5
A2	49.41	682	52.75	2.03×10^{11}	4.65×10^5
B1	48.40	668	51.65	1.86×10^{11}	4.46×10^5
B2	46.57	709	49.73	2.36×10^{11}	5.02×10^5

TABLE III. The glueball masses (in MeV) obtained in our model, compared against the results of IHQCD [4] and lattice QCD [51]. The first two values of masses for 0^{++} and 0^{++*} are used as input data in our procedure. The results here were obtained with $\epsilon = 0.01$.

n	A1	A2	B1	B2	IHQCD [4]	Lattice [51]
0^{++}	1475	1475	1475	1475	1475	1475(30)(65)
0^{++*}	2755	2755	2755	2755	2753	2755(70)(120)
0^{++**}	3507	3376	3361	3449	3561	3370(100)(150)
0^{++***}	4106	3891	3861	4019	4253	3990(210)(180)
0^{++****}	4621	4349	4313	4514	4860	
$0^{++*****}$	5079	4762	4721	4956	5416	
2^{++}	2075	2180	2182	2130	2055	2150(30)(100)
2^{++*}	2945	2899	2887	2943	2991	2880(100)(130)
2^{++**}	3619	3468	3444	3568	3739	
2^{++***}	4185	3962	3928	4102	4396	
2^{++****}	4680	4404	4365	4576	5530	
$2^{++*****}$	5127	4807	4763	5006		

$$m_{t,n}^2 = \Lambda^2(8.13n + 7.92), \qquad n = 0, 1, 2, \ldots \tag{103}$$

The largest difference between the masses obtained with these fits and the lattice QCD results occurs for the state 0^{++} and is of about 10%.

The same procedure was done for model A2, where the dilaton is given by Eq. (76), and for $\epsilon = 0.01$ the values $\hat{\phi}_0 = 49.41$ and $\Lambda = 682$ MeV were found. The other parameters are displayed in Table II.

The mass spectrum obtained in model A2 is shown in the third column of Table III. We find again a good agreement between our results and those of the lattice QCD [51] and the IHQCD model [4]. In comparison to the lattice QCD masses, the largest difference is of about 2.4% in the case of $m_{0^{++***}}$.

The spectrum of model A2 is also well approximated by linear fits. The linear trajectories in this case are

$$m_{s,n}^2 = \Lambda^2(8.62n + 6.37), \qquad n = 0, 1, 2, \ldots \tag{104}$$

for the scalar sector and

$$m_{t,n}^2 = \Lambda^2(7.89n + 10.16), \qquad n = 0, 1, 2, \ldots \tag{105}$$

for the tensor sector. When compared to the lattice QCD results, the maximum error obtained for these fits is of about 16.8%, and it occurs for the state 0^{++}.

2. Models B

The two models we named B1 and B2 are described in Appendix B and correspond to the case where the warp factor $A(z)$ has an analytic form, while the dilaton is solved numerically from the first equation in (20).

The parameters obtained for models B1 and B2 at $\epsilon = 0.01$ are shown in the third and fourth rows of

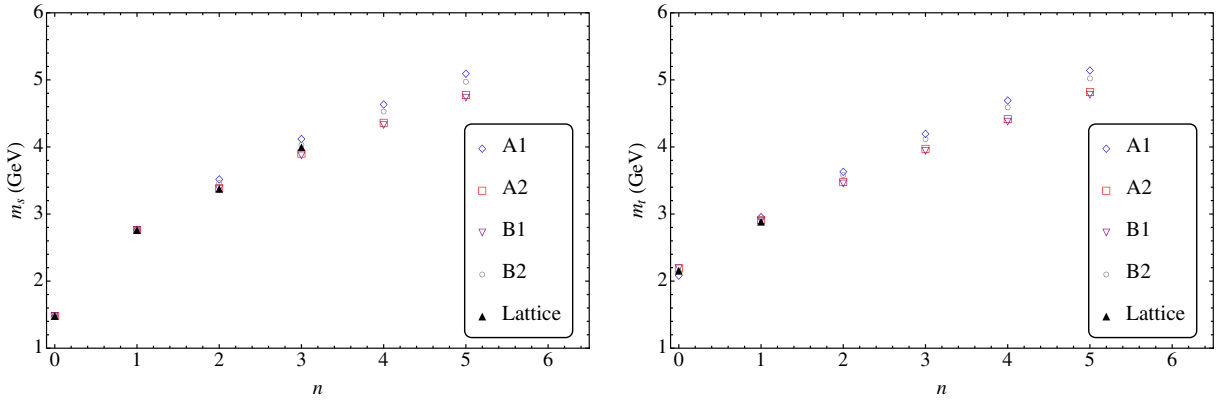

FIG. 5. The glueball spectrum for the scalar (left panel) and tensor (right panel) sectors obtained in models A1, A2, B1, and B2 at $\epsilon = 0.01$, compared against lattice QCD data [51].

Table II. The glueball spectra obtained for models B1 and B2 are shown in the fourth and fifth columns of Table III. The numerical results for models B1 and B2 are also in good agreement with the lattice QCD and IHQCD model. The approximate linear trajectories for model B1 are

$$m_{s,n}^2 = \Lambda^2(8.80n + 6.74),$$
$$m_{t,n}^2 = \Lambda^2(8.04n + 10.62), \qquad n = 0, 1, 2, \ldots, \quad (106)$$

while for model B2 we obtain

$$m_{s,n}^2 = \Lambda^2(8.80n + 5.47),$$
$$m_{t,n}^2 = \Lambda^2(8.17n + 9.03), \qquad n = 0, 1, 2, \ldots. \quad (107)$$

In Fig. 5 we plot the results for the spectra of scalar and tensor glueballs obtained in the four models considered in this work (A1, A2, B1 and B2) and, for comparison, we include the data of lattice QCD [51]. The results for models A1 and B1 are shown in Fig. 6. The plots show clearly the pattern $m_{s,n} < m_{t,n}$, also observed in the IHQCD model [4]. Notice that the difference between the scalar and tensor glueball masses decreases as n increases. This indicates a degeneracy of the scalar and tensor glueballs at very large n.

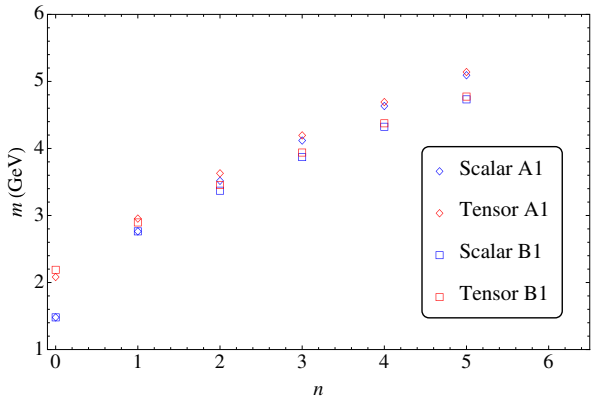

FIG. 6. The scalar and tensor glueball spectrum for models A1 and B1 at $\epsilon = 0.01$.

D. Running parameters

So far in this section, all the calculations were done for a specific value of the conformal dimension, $\epsilon = 0.01$. But what happens when this parameter varies? Here we find the evolution of the parameters $\hat{\phi}_0$ and Λ with the conformal dimension ϵ for models A1 and A2. As explained previously in this section, for any given ϵ we use the masses of the first two scalar glueballs, extracted from lattice QCD, as an input for fixing $\hat{\phi}_0$ and Λ.

The results for $\hat{\phi}_0$ are displayed on the left panel of Fig. 7. A numerical fit shows that $\hat{\phi}_0$ diverges as $1/\epsilon$ as the parameter ϵ goes to 0. The evolution of Λ with ϵ is shown on the right panel of Fig. 7. The evolution is very slow suggesting that Λ should be approximated by a constant. Linear fits for these results give $\Lambda = 735.18 + 75.48\epsilon$ for model A1 and $\Lambda = 682.27 - 43.22\epsilon$ for model A2, both in MeV units.

Additionally, we find the evolution of the parameters ϕ_0 and G, related to $\hat{\phi}_0$ and Λ by Eq. (65). The results for ϕ_0 are shown on the left panel of Fig. 8. A fit for model A1 gives $\phi_0 = 4.47 + 0.53/\epsilon$, while for model A2 one finds $\phi_0 = 4.42 + 0.49/\epsilon$ (both in MeV$^\epsilon$ units). The evolution of the parameter G is displayed on the right panel of Fig. 8. A numerical fit of the data corresponding to such figures, shows that, when ϵ goes to 0, G reaches a finite value: 2.92×10^{11} MeV^4 for model A1 and 2.16×10^{11} MeV^4 for model A2.

We have also obtained numerically the vacuum energy density, given by (83). The results are shown in Fig. 9 where we have set $(M_p\ell)^3 N_c^2$ to 1. One clearly sees that the vacuum energy density converges to a finite value when ϵ goes to 0. This can be understood as follows. We showed previously that, when ϵ goes to 0, the source ϕ_0 goes as

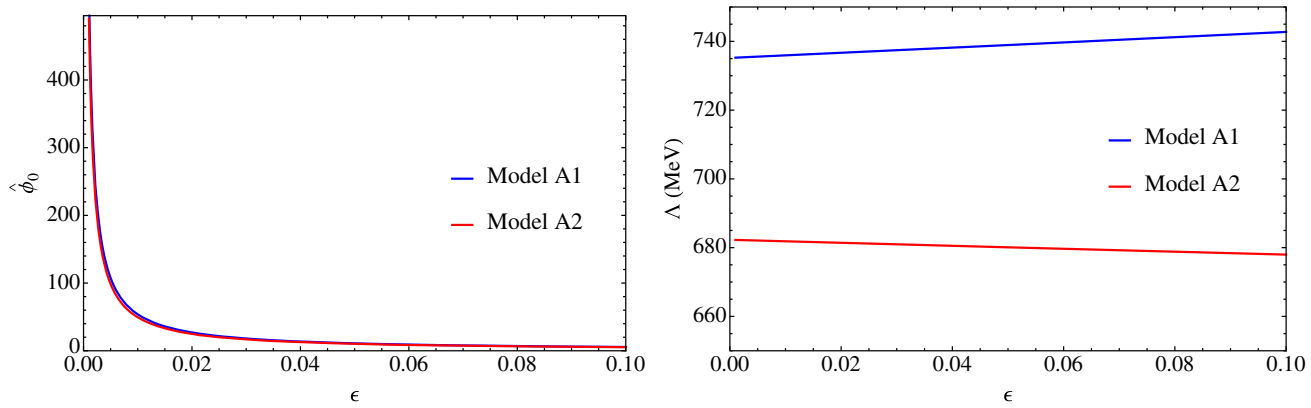

FIG. 7. Evolution of the parameters $\hat{\phi}_0$ (left panel) and Λ (right panel) with the conformal dimension ϵ for models A1 and A2.

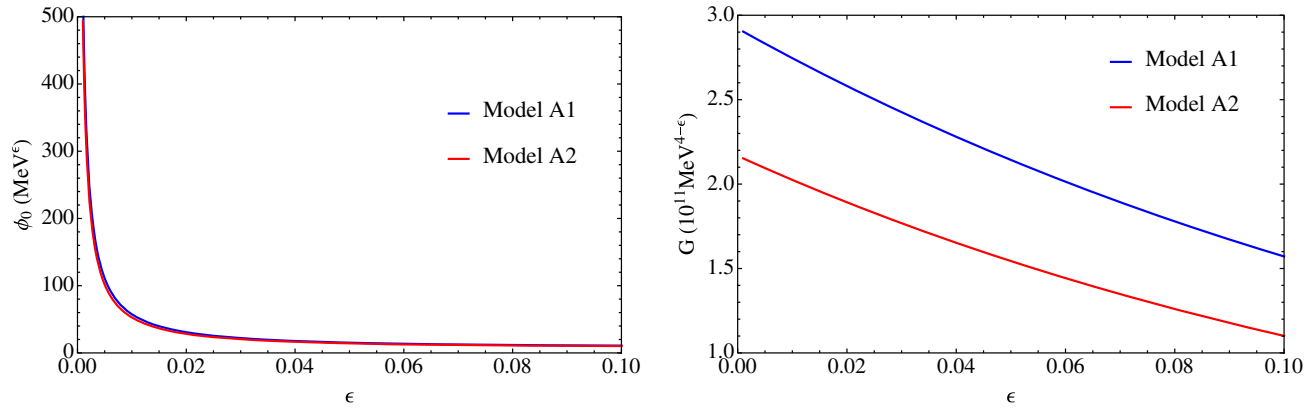

FIG. 8. Evolution of the parameters ϕ_0 (left panel) and G (right panel) with the conformal dimension ϵ for models A1 and A2.

$c_1 + c_2/\epsilon$. Therefore, the renormalized vacuum energy density ($\mathcal{E}^{ren}_{\rm QCD} \propto \epsilon\phi_0$) goes as $c_2 + c_1\epsilon$. The numerical results shown in Fig. 9 indicate that the vacuum energy density evolves very slowly with the conformal dimension ϵ, in both models A1 and A2, and can be approximated by a constant. Our predictions for $\mathcal{E}^{ren}_{\rm QCD}$, in the limit $\epsilon \to 0$, are

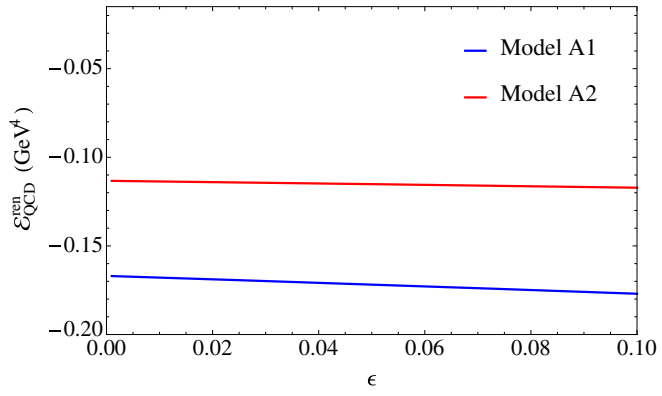

FIG. 9. Evolution of the renormalized vacuum energy density $\mathcal{E}^{ren}_{\rm QCD}$ with the conformal dimension ϵ for models A1 and A2. We have set $(M_p\ell)^3N_c^2$ to 1.

-0.17 GeV^4 in model A1, and -0.11 GeV^4 in model A2. We remark that we have set $(M_p\ell)^3N_c^2$ to 1. For comparison, an analysis made in [52], by considering the large-N_c limit, led to $\mathcal{E}_{\rm QCD} = -c_0^4N_c^2\sigma_0^2$, where σ_0 is the QCD string tension and c_0 is a constant of order 1. Considering a phenomenological value for the string tension, e.g. $\sigma_0 = (0.44\ \text{GeV})^2$ [53], and taking $N_c = 3$ and $c_0 = 1$ one gets $\mathcal{E}_{\rm QCD} \approx -0.34$ GeV^4.

V. THE TRACE ANOMALY: FROM DEFORMED CFTS TO QCD

In this section we take advantage of the AdS/CFT dictionary and reproduce the universal result for the trace anomaly of deformed CFTs [9,14] for the particular backgrounds considered in this work. This result in turn suggests a map between deformed CFTs and large-N_c QCD. An important ingredient in this map is the reinterpretation of the CFT deformation $\delta\mathcal{L} = \phi_0\mathcal{O}$ in terms of the large-N_c Yang-Mills Lagrangian $\mathcal{L}_{\rm YM}$.

In Euclidean signature the large-N_c Yang-Mills Lagrangian can be written as [54]

$$\mathcal{L}_{\rm YM} = N_c\bar{\mathcal{L}}_{\rm YM}, \tag{108}$$

with

$$\bar{\mathcal{L}}_{\rm YM} = \frac{1}{\lambda}\left(\frac{1}{2}{\rm Tr}F^2\right). \tag{109}$$

Here we can make use of the mass parameter Λ, defined previously in (65), which has conformal dimension 1. Multiplying and dividing Eq. (109) by Λ^ϵ, we get

$$\bar{\mathcal{L}}_{\rm YM} = \frac{\Lambda^\epsilon}{\lambda}\left(\frac{1}{2}\frac{{\rm Tr}F^2}{\Lambda^\epsilon}\right). \tag{110}$$

In this way we have dressed the inverse 't Hooft coupling $1/\lambda$ and the QCD operator $\frac{1}{2}{\rm Tr}F^2$ so that they acquire conformal dimensions ϵ and $4-\epsilon$, respectively. Matching the Lagrangian $\bar{\mathcal{L}}_{\rm YM}$ to the CFT deformation $\delta\mathcal{L} = \phi_0\mathcal{O}$, we obtain the map

$$\phi_0 = \frac{\Lambda^\epsilon}{\lambda}, \qquad \mathcal{O} = \frac{1}{2}\frac{{\rm Tr}F^2}{\Lambda^\epsilon}. \tag{111}$$

Below we use this map for calculating the gluon condensate and to find a connection between the trace anomaly of deformed CFTs and the QCD trace anomaly.

A. The gluon condensate

According to the AdS/CFT dictionary the VEV of an operator $\mathcal{O}$ is obtained from the variation of the on-shell action [9,14,20,21]

$$\delta S^{o-s} = \int d^4x\delta\phi_0\langle\mathcal{O}\rangle, \tag{112}$$

where $\delta\phi_0$ is the variation of the source. In the case of holographic QCD backgrounds, the on-shell action was obtained in Sec. III D with the result

$$S^{\rm o-s} = 6M_p^3N_c^2\int d^4x e^{3A(z_0)}A'(z_0), \tag{113}$$

with small z_0 and, as usual, the limit $z_0\to 0$ is taken at the very end of the calculation process. We then variate this on-shell action by considering the warp factor A as a field whose dynamics is completely determined by the dilaton field Φ, $A = A(\Phi)$. Therefore, we get

$$\begin{aligned}\delta S^{\rm o-s} &= 6M_p^3N_c^2\int d^4x\delta\Phi\frac{d}{d\Phi}[e^{3A(z_0)}A'(z_0)]\\ &= 6M_p^3N_c^2\int d^4x\delta\phi_0 z_0^\epsilon\frac{1}{\Phi'(z_0)}\frac{d}{dz_0}[e^{3A(z_0)}A'(z_0)],\end{aligned} \tag{114}$$

where we used the asymptotic form of the dilaton (64) to rewrite Φ in terms of the source ϕ_0. From Eqs. (112) and (114) we find the bare VEV of the operator $\mathcal{O}$,

$$\langle\mathcal{O}\rangle = 6M_p^3N_c^2z_0^\epsilon\frac{1}{\Phi'(z_0)}e^{3A(z_0)}[A''(z_0)+3A'^2(z_0)]. \tag{115}$$

Using the field equations (20) and the definition (24), we may rewrite this VEV as

$$\langle\mathcal{O}\rangle = 24M_p^3N_c^2z_0^\epsilon e^{3A(z_0)}\frac{A'(z_0)}{3X(z_0)}[1-X^2(z_0)]. \tag{116}$$

As it was done previously for the case of the bare energy density, we use the UV asymptotic form of A and X to identify the divergent and nondivergent terms in (116). Again, we consider a MS scheme for renormalization. Eliminating the divergent terms and taking the $z_0\to 0$ limit, we obtain the renormalized VEV,

$$\langle\mathcal{O}\rangle^{ren} = \frac{16}{15}(M_p\ell)^3N_c^2(4-\epsilon)G. \tag{117}$$

Using the map (111) and the definitions in (65), we find the gluon condensate

$$\langle{\rm Tr}F^2\rangle^{ren} = \frac{32}{15}(M_p\ell)^3N_c^2(4-\epsilon)\Lambda^4. \tag{118}$$

In Fig. 10 we plot our numerical results for the gluon condensate $\langle\frac{1}{4\pi^2}{\rm Tr}F^2\rangle^{ren}$ as a function of ϵ for models A1 and A2, where we have set $(M_p\ell)^3N_c^2$ to 1. We remark that the gluon condensate in (118) was obtained in a particular renormalization scheme. Taking the limit $\epsilon\to 0$, the results for the gluon condensate $\langle\frac{1}{4\pi^2}{\rm Tr}F^2\rangle^{ren}$ are 0.063 and 0.047 GeV^4 for models A1 and A2, respectively. For comparison, we present other results in the literature. The values obtained using Shifman-Vainshtein-Zakharov sum

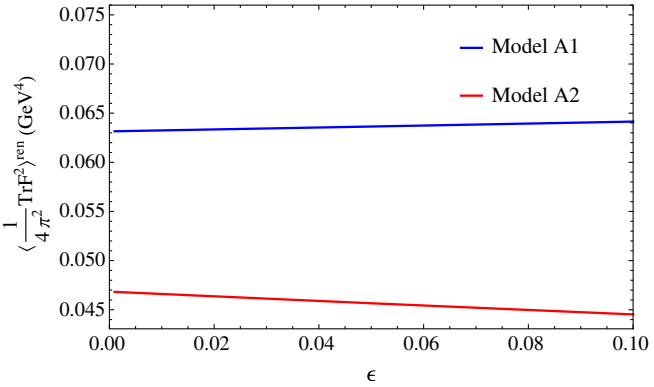

FIG. 10. Evolution of the renormalized gluon condensate $\langle\frac{1}{4\pi^2}{\rm Tr}F^2\rangle^{ren}$ with the conformal dimension ϵ for models A1 and A2. We have set $(M_p\ell)^3N_c^2$ to 1.

rules are 0.013 [55] and 0.012 GeV^4 [56]. Previous results in holographic QCD include 0.043 [2] and 0.01 GeV^4 [57]. We also mention two different results in SU(3) lattice gauge theory: 0.10 [58] and 0.04 GeV^4 [59].

B. The trace anomaly

The renormalized vacuum energy density $\mathcal{E}^{ren}_{\rm QCD}$ for our model is given by Eq. (83). At zero temperature, the pressure is just $-\mathcal{E}^{ren}_{\rm QCD}$, so the trace of the energy-momentum tensor is given by

$$\langle T^{\mu}{}_{\mu}\rangle^{ren} = 4\mathcal{E}^{ren}_{\rm QCD} = -\frac{16}{15}(M_p\ell)^3 N_c^2 \epsilon(4-\epsilon)\phi_0 G. \quad (119)$$

From Eqs. (117) and (119), we find the relation

$$\langle T^{\mu}{}_{\mu}\rangle^{ren} = -\epsilon\phi_0\langle\mathcal{O}\rangle^{ren}. \quad (120)$$

This is the universal trace anomaly of four-dimensional CFTs deformed by an operator $\mathcal{O}$ with dimension $\Delta = 4-\epsilon$ and coupling ϕ_0 [9,14]. The quantity $-\epsilon\phi_0$ is the classical β function associated with the coupling ϕ_0. We have reproduced this trace anomaly within the context of effective holographic QCD backgrounds, where the dilaton and warp factor depend solely on the radial coordinate z. This trace anomaly describes the explicit breaking of conformal symmetry and, as described in the previous section, a nontrivial consequence of this symmetry breaking is the discrete spectrum of scalar and tensor glueballs. It is interesting to note that the limit $\epsilon \to 0$, with ϕ_0 fixed, corresponds to the case where conformal symmetry is spontaneously broken. In that case, as explained in Appendix A, the first scalar glueball becomes a Nambu-Goldstone boson.

The trace anomaly (120) holds for more general backgrounds where the dilaton and metric are more involved. In any case the conformal dimension of $\mathcal{O}$ always maps to a mass term for the dilaton via the relation $M^2\ell^2 = \Delta(\Delta-4)$. Although a general proof of (120) was developed in [9,14], it is always illuminating to reproduce this trace anomaly case by case. In particular, it would be interesting to prove (120) for the case of black hole solutions, such as those considered in [6,7].

We finish this section proposing a dictionary between the conformal trace anomaly (120) and the QCD trace anomaly. Making use of the map (111) we can rewrite (120) as

$$\langle T^{\mu}{}_{\mu}\rangle^{ren} = -\frac{\epsilon}{2\lambda}\langle {\rm Tr}F^2\rangle^{ren}. \quad (121)$$

This result looks very similar to the QCD trace anomaly

$$\langle T^{\mu}{}_{\mu}\rangle^{ren} = \frac{\beta}{2\lambda^2}\langle {\rm Tr}F^2\rangle^{ren}, \quad (122)$$

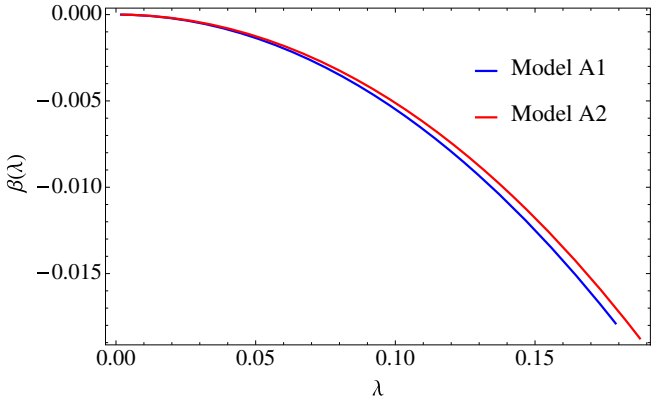

FIG. 11. The four-dimensional β function in terms of λ, for models A1 and A2, obtained from the dictionary proposed in this section.

suggesting the identification $\epsilon = -\beta/\lambda$. We remind the reader that the CFT deformation takes place at some UV energy scale μ^* so the coupling λ appearing in Eq. (121) is actually evaluated at that scale.

A few remarks are in order here. The dictionary proposed in this work differs from the original proposal [6,7] because we map the conformal dimension ϵ to the β function of the four-dimensional theory, instead of the anomalous dimension of ${\rm Tr}F^2$. Our approach also differs from [3,4] where the four-dimensional β function is mapped to the five-dimensional field X. In [3,4] the four-dimensional RG energy scale μ and coupling λ are mapped to the five-dimensional warp factor $A(z)$ and dilaton $\Phi(z)$ in a very natural way. However, evaluating correlation functions at any RG energy scale μ^* appears to be a difficult task due to the necessity of introducing a geometric cutoff z^*.[7] In the effective holographic approach considered here, although the dictionary proposed in [3,4] can still be used, we have to distinguish between the β function and RG energy scale of the effective theory and the QCD β function and RG energy scale. In particular, approaching a UV cutoff μ^* in the QCD RG energy scale corresponds to the limit $\mu \to \infty$ in the effective theory. While the QCD β function does not vanish there, it is mapped to the conformal dimension ϵ, the effective theory β function goes to 0 because we approach a CFT fixed point. Moreover, in our approach a QCD RG energy cutoff μ^* does not imply cutting the five-dimensional geometry so that one can make use of the usual AdS/CFT dictionary by embedding holographic QCD in the framework of holographic deformed CFTs, developed in [8,9,14].

Figure 11 shows the numerical results for the emergent QCD β function in terms of λ. According to the dictionary proposed in this work, these quantities are identified with $-\epsilon/\hat{\phi}_0$ and $1/\hat{\phi}_0$, respectively. We made a numerical

[7]See, however, the recent progress made in [29].

fit for small λ and interestingly the fit takes the form $\beta = -b_0\lambda^2 - b_1\lambda^3$. This is the same form arising in large-N_c perturbative QCD at two loops, with b_0 and b_1 being scheme independent. For model A1 we find $b_0 \approx 0.54$ and $b_1 \approx 0.48 b_0^2$, while for model A2 we obtain $b_0 \approx 0.49$ and $b_1 \approx 1.04 b_0^2$. For comparison, the coefficients of the large-N_c perturbative QCD β function are $b_0 \approx 0.046$ and $b_1 \approx 0.42 b_0^2$.

We finish this section describing the relation between the anomalous dimension $\epsilon_{\rm an}$ of $\mathrm{Tr}F^2$ and the conformal dimension ϵ. Following Ref. [7], the anomalous dimension $\epsilon_{\rm an}$ can be extracted from the QCD trace anomaly (122) with the result

$$\epsilon_{\rm an} = -\lambda^2 \partial_\lambda [\beta \lambda^{-2}]. \tag{123}$$

At small λ the anomalous dimension (123) is approximated by $\epsilon_{\rm an} \approx b_1 \lambda^2$. Using the identifications proposed in this work, namely $\hat{\phi}_0 = \frac{1}{\lambda}$ and $\epsilon = -\frac{\beta}{\lambda}$, this relation becomes

$$\epsilon_{\rm an} = \partial_{\hat{\phi}_0}[-\epsilon \hat{\phi}_0] = \partial_{\hat{\phi}_0}\beta_{\hat{\phi}_0}, \tag{124}$$

where in the last equality we have introduced the beta function associated with $\hat{\phi}_0$, defined as the derivative of $\hat{\phi}_0$ with respect to $\log \mu^*$. Interestingly, the relation (124) looks very similar to the anomalous dimensions that arise in holographic RG flows [60].

VI. CONCLUSIONS

In this work we have investigated effective holographic models where QCD is described in terms of a four-dimensional CFT deformation. The deformation is of the form $\delta\mathcal{L} = \phi_0 \mathcal{O}$, where $\mathcal{O}$ is a relevant operator and ϕ_0 the coupling, and takes place at a UV energy scale μ^*. It is characterized by the conformal dimension of the relevant operator $\Delta = 4 - \epsilon$, which according to the AdS/CFT dictionary maps to the five-dimensional mass of the dual dilaton field. The IR dilaton asymptotics was constrained by the criteria of confinement and linear glueball spectrum, namely a dilaton quadratic in the radial coordinate z. We have proposed UV/IR semianalytic interpolations that lead to a spectrum of scalar and tensor glueballs consistent with lattice QCD. A key ingredient in our description was the evolution of the model parameters with ϵ. In particular, the evolution of the coupling ϕ_0 with ϵ was essential to guarantee an explicit breaking of conformal symmetry consistent with the glueball spectrum.

Making use of the AdS/CFT correspondence we have evaluated the renormalized vacuum energy density $\langle T^{00}\rangle^{ren}$ and the VEV of the relevant operator $\langle \mathcal{O}\rangle^{ren}$ in the four-dimensional theory. Both quantities are different from 0 as a consequence of the CFT deformation. We have mapped those quantities to the QCD vacuum energy and gluon condensate respectively. We have also reproduced the universal result for the trace anomaly in four-dimensional deformed CFTs, namely $\langle T^{\mu}{}_{\mu}\rangle^{ren} = -\epsilon\phi_0\langle\mathcal{O}\rangle^{ren}$, and reinterpreted this result in terms of the QCD trace anomaly. This led us to suggest a map between the conformal dimension ϵ and the β function of the QCD-like theory. The dictionary found in this work differs from the one proposed in [3,4], but establishes a novel connection between QCD and deformed CFTs. Moreover, from the evolution of ϕ_0 with ϵ and the dictionary proposed in this work we found a four-dimensional emergent β function that behaves qualitatively as the large-N_c QCD β function in the perturbative regime. This nontrivial result indicates that the holographic description of QCD as a CFT deformation can be consistent with asymptotic freedom without the necessity of building a specific potential.

There are some pieces of the dictionary that remain to be found, such as a more precise relation between the five-dimensional warp factor and the four-dimensional RG energy of the QCD-like theory. As described in the previous section, although the dictionary proposed in [3,4] could still be used to extract the RG energy scale of the effective theory the challenge is to map this to the RG energy scale of the original QCD-like theory. A map between the backgrounds developed in this work and the backgrounds developed in [3,4] would also be desirable. That map should be such that the metric and dilaton near a geometric cutoff z^* in the background of [3,4] becomes an AdS metric slightly deformed by a massive dilaton. The holographic description of the Callan-Symanzik equations, following [29,60], would also shed some light on the connection between holographic QCD and deformed CFTs.

We finish this work mentioning some of its possible extensions. The description of mesons and chiral symmetry breaking in terms of gauge fields and a tachyonic field can be done, inspired by the progress made in [5,61,62]. Investigating black hole solutions at finite temperature will allow the description of a nonconformal plasma, complementing the progress made in [6,7,63]. In this context, a particularly interesting phenomenon is the so-called glueball melting [64]. Finally, the study of higher spin glueballs and the pomeron could be pursued, along the lines of [65] and more recently [49,66–68].

ACKNOWLEDGMENTS

The authors acknowledge conversations and correspondence with Nelson R. F. Braga, Renato Critelli, Stefano Finazzo, Elias Kiritsis, Carlisson Miller, Jorge Noronha and Robert C. Quevedo. This work was partially funded by Fundação de Amparo à Pesquisa do Estado de São Paulo (FAPESP), Brazil, Grants No. 2011/18729-1 (V. T. Z.), No. 2013/17642-5 (L. A. H. M.) and No. 2015/17609-3 (A. B.-B.). V. T. Z. also thanks Coordenação de Aperfeiçoamento do Pessoal de Nível Superior (CAPES), Brazil, Grant No. 88881.064999/2014-01, and Conselho

Nacional de Desenvolvimento Científico e Tecnológico (CNPq), Brazil, Grant No. 308346/2015-7. A. B.-B. also acknowledges partial financial support from Grant No. CERN/FIS-NUC/0045/2015. H. B. F. also acknowledges partial financial support from CNPq Grant No. 307278/2015-8.

APPENDIX A: THE MASSLESS MODE IN THE SCALAR SECTOR

In this appendix we develop a semianalytic approach to treat the massless mode; additionally we are setting the AdS radius to be 1, $\ell = 1$. We find general criteria to identify whether a massless mode appears or not. Such an approach follows the same idea of Refs. [4,24]. The starting point is the Schrödinger-like Eq. (52), which can be written as [4,24]

$$P^\dagger P\psi_s(z) = \hat{m}_s^2\psi_s(z), \tag{A1}$$

where $P = -\partial_z + B_s'(z)$ and $P^\dagger = \partial_z + B_s'(z)$.

Our goal here is to prove that there is a massless state with normalizable wave function in the bulk. In order to do that, we need the asymptotic expansions of the dilaton in the UV and IR regimes, which are respectively of the form

$$\begin{aligned}\Phi(z) &= \phi_0 z^{\Delta_-} + Gz^{\Delta_+}, \qquad z \to 0,\\ \Phi(z) &= Cz^2, \qquad z \to \infty,\end{aligned} \tag{A2}$$

where $\Delta_+ = 4 - \Delta_-$.

Since we are looking for the wave function of the massless mode, we substitute $\hat{m}_s^2 = 0$ in Eq. (A1) to get

$$[\partial_z + B_s'(z)][-\partial_z + B_s'(z)]\psi_s(z) = 0. \tag{A3}$$

The solutions of this equation may be written as [24]

$$\psi_s^{(1)}(z) = e^{B_s(z)}, \quad \psi_s^{(2)}(z) = e^{B_s(z)}\int_0^z e^{-2B_s(z')}dz'. \tag{A4}$$

The next step is to verify the normalizability of such solutions, which means that the integral

$$I = \int_0^\infty dz\psi_s(z)\psi_s^*(z) \tag{A5}$$

must be finite. Following the procedure developed in Sec. IV A, we write down the leading terms of the asymptotic expansions for $B_s(z)$ in the UV and IR regimes,

$$B_s(z) = \log\left[\frac{1}{3}\phi_0\Delta_- z^{(\Delta_- - 3/2)} + \frac{1}{3}G\Delta_+ z^{(\Delta_+ - 3/2)} + \cdots\right], \quad z \to 0; \tag{A6a}$$

$$B_s(z) = -Cz^2 + \cdots, \qquad z \to \infty; \tag{A6b}$$

where ϕ_0, G and C are the constant parameters previously introduced, with C being a positive real parameter.

We start by analyzing the first solution, $\psi_s^{(1)}(z)$, in the IR regime. Using Eqs. (A4), (A5) and (A6), we conclude that the first solution is normalizable. In fact, one has in this case the solution $\psi_s^{(1)}(z) = e^{-Cz^2}$, so the integral (A5) is finite in the IR.

We now analyze the first solution in the UV regime. In such a limit, this solution can be written as

$$\psi_s^{(1)}(z) = c_1 z^{(-3/2+\Delta_-)} + c_2 z^{(5/2-\Delta_-)}, \quad \text{where}$$
$$c_1 = \frac{1}{3}\Delta_-\phi_0, \qquad c_2 = \frac{1}{3}\Delta_+ G. \tag{A7}$$

We see that the coefficients c_1 and c_2 in Eq. (A7) are related to the source ϕ_0 and to the condensate G, respectively.

Considering the solutions of equation $\Delta(\Delta - 4) = M^2$, and taking into account the Breitenlohner-Freedman bound [69], $0 \le \Delta_- \le 2$ and $2 \le \Delta_+ \le 4$, we have the following four possibilities.

(1) $\Delta_- = 0$ and $\Delta_+ = 4$. This represents the extremal case, for which $M = 0$. In this case the conformal dimension does not show, but there are still the source and the condensate, the last effect being responsible for the spontaneous break of the conformal symmetry. The dilaton expansion in the UV becomes

$$\Phi(z) = \phi_0 + Gz^4, \qquad z \to 0. \tag{A8}$$

By using the result (A7), the solution in the UV becomes $\psi_s^{(1)}(z) = 4Gz^{5/2}/3$. This means the integral (A5) is finite in the UV. It follows that the solution is normalizable in the UV limit. Then, there exists a massless mode in the extremal case, as previously studied by Csaki and Reece [2].

(2) $0 < \Delta_- < 1$ and $3 \le \Delta_+ < 4$. In this case the first term in (A7) is divergent close the boundary unless its coefficient is 0 (after the integration). This means that the source should be turned off, $\phi_0 = 0$, in order to have a resulting normalizable wave function. This means that we are breaking explicitly the conformal symmetry (because $\Delta_+ = 4 - \Delta_-$), but the massless mode is present since the corresponding wave function is normalizable from the UV to the IR limit in the bulk. However, if the source is turned on, the wave function becomes non-normalizable, i.e., the integral diverges. The conclusion is that there is no massless mode in the presence of a source. In the case studied in this work, we have a small

deformation $\Delta_- = \epsilon$ that we are interpreting as conformal dimension, and the source is turned on. This explains why there are no massless modes in the analysis of Sec. IV. At this point it is worth emphasizing that we must have both, source and deformation, to eliminate the massless mode.

(3) Now let us look at the case $\Delta_- = 1$ and $\Delta_+ = 3$. The solution (A7) becomes $\psi_s^{(1)}(z) = c_1 z^{-1/2} + c_2 z^{3/2}$. The analytical model presented in Appendix G of Ref. [4] is included here as a particular case with $\Delta_- = 1$ and $\phi_0 \neq 0$. As seen in the above analysis, there exists a massless mode if we turn off the source, i.e., $c_1 = 0$, and there are no massless modes when the source is turned on. An alternative analysis of this case, studying nearly marginal operators, was developed in [15].

(4) $1 < \Delta_- \leq 2$ and $2 \leq \Delta_+ < 3$. According to the exponent in the solution (A7) there are three situations to be considered.

(a) $1 < \Delta_- < 3/2$ and $5/2 < \Delta_+ < 3$. In this case the integral (A5) converges in the UV. Therefore, there is a massless mode for these ranges of $\Delta_\pm$ values.

(b) $\Delta_- = 3/2$ and $\Delta_+ = 5/2$. For these specific values of $\Delta_\pm$, the integral is a constant that depends on the source value (which is finite) and therefore the wave function is normalizable. So, there is a massless mode also for these specific values of $\Delta_\pm$.

(c) $3/2 < \Delta_- \leq 2$ and $2 \leq \Delta_+ < 5/2$. In this case the integral (A5) converges (as $z \to 0$). Therefore, there is a massless mode.

As the integral is always finite in case iv, it means that both terms of the wave function (A7) are normalizable, and the source and the condensate can exchange their roles [16].

Now let us look at the second solution, $\psi_s^{(2)}(z)$. In the IR regime we have

$$\psi_s^{(2)}(z) = e^{-Cz^2} \int e^{2Cz^2} dz = \frac{1}{2}\sqrt{\frac{\pi}{2C}} e^{-Cz^2} \mathrm{Erfi}[\sqrt{2C}z], \tag{A9}$$

where $\mathrm{Erfi}[\sqrt{2C}z]$ is the imaginary error function. The last term in the above equation is divergent. Then the wave function is non-normalizable. On the other hand, in the UV regime we have

$$\psi_s^{(2)}(z) = e^{(\Delta_- - 3/2)\log z} \int_0^z e^{-2(\Delta_- - 3/2)\log z'} dz'. \tag{A10}$$

This solution may or may not be normalizable in the UV. But as the solution in the IR is always non-normalizable, there is not a massless mode in this case.

In conclusion, the normalizability of the first solution $\psi_s^{(1)}(z)$ depends on the values of Δ_- and ϕ_0. As this solution is normalizable in the IR, by choosing appropriately these two parameters, it can be made normalizable also in the UV regime, and then a massless mode can be obtained in this case. On the other hand, the second solution is non-normalizable in the IR. This result excludes the possibility of getting a massless mode from the second solution.

APPENDIX B: MODELS B: ANALYTIC FORM FOR THE WARP FACTOR

Alternatively to what was presented in the main body of this work, we can choose to interpolate the warp factor between the UV and IR, instead of the dilaton. An analytic warp factor is useful when exploring finite temperature effects. We call this approach to interpolating the warp factor model B. Inspired by the interpolations done above for the dilaton field, we carefully seek the form of the interpolating functions so that they produce the asymptotic forms of Eqs. (59) and (67), respectively.

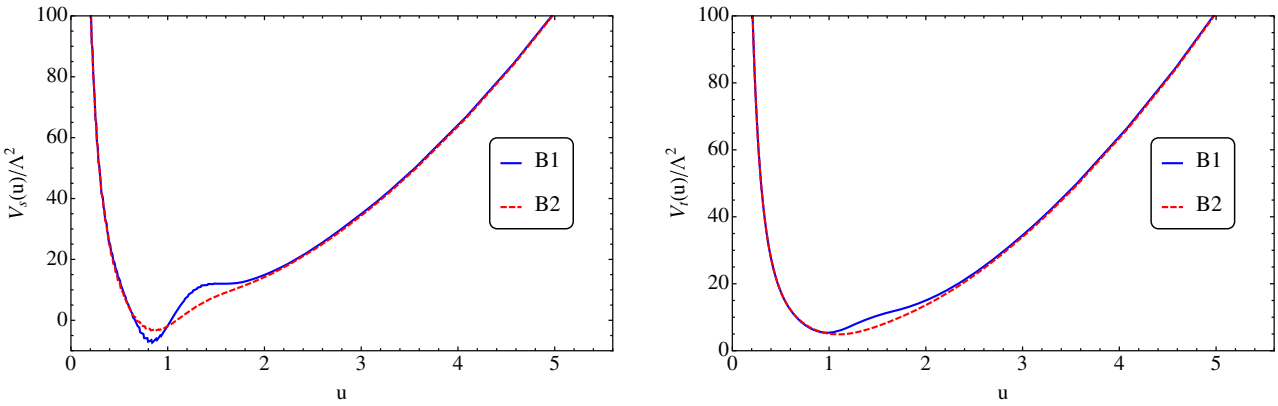

FIG. 12. The scalar (left panel) and tensor (right panel) normalized potentials for $\epsilon = 0.01$ and $\hat{\phi}_0 = 50$, in models B1 and B2.

Our first choice, motivated by model A1, is

$$A(z) = -\log(z/\ell) - \frac{2\epsilon\phi_0^2}{9(1+2\epsilon)} z^{2\epsilon} - \frac{2\epsilon(4-\epsilon)\phi_0\Lambda^{4-\epsilon}}{45} \times \frac{z^4}{1+a_1(z)} - \frac{(\Lambda z)^{8-2\epsilon}}{\frac{9(9-2\epsilon)}{2(4-\epsilon)} + b_1(z)}, \quad \text{(B1)}$$

where the functions $a_1(z) = 7(\Lambda z)^5/50$ and $b_1(z) = 5(\Lambda z)^4 + 3(\Lambda z)^{6-2\epsilon}/2$ were introduced to guarantee the compatibility of the results of the model with those of the lattice QCD [51]. These functions also guarantee that the warp factor decreases monotonically from the UV to the IR, as required in dilaton-gravity models [24]. We named this interpolation form model B1.

The second model, called B2, that produces the asymptotic forms of Eqs. (59) and (67), respectively, is inspired by model A2. The chosen warp factor is

$$A(z) = -\log(z/\ell) - \frac{2\epsilon\phi_0^2}{9(1+2\epsilon)} z^{2\epsilon} - \frac{2\epsilon(4-\epsilon)\phi_0\Lambda^{4-\epsilon}}{45} \frac{z^4}{1+a_2(z)} - \frac{(\Lambda z)^6 \tanh^2[(\Lambda z)^{1-\epsilon}]}{\frac{9(9-2\epsilon)}{2(4-\epsilon)} + b_2(z)}. \quad \text{(B2)}$$

As before, the functions $a_2(z) = 7(\Lambda z)^4/50$ and $b_2(z) = 733(\Lambda z)^2/100 + 3(\Lambda z)^4/2$ were adjusted to get compatible results with those of the lattice QCD [51], and to yield a monotonically decreasing warp factor.

To complete the analysis of these models, we show in Fig. 12 the potentials of the Schrödinger-like equations for both sectors, scalar and tensor, as indicated. The spectra calculated using these models are presented in Table III.

[1] E. V. Shuryak, Lect. Notes Phys. **71**, 1 (2004); **8**, 1 (1988).
[2] C. Csaki and M. Reece, J. High Energy Phys. 05 (2007) 062.
[3] U. Gursoy and E. Kiritsis, J. High Energy Phys. 02 (2008) 032.
[4] U. Gursoy, E. Kiritsis, and F. Nitti, J. High Energy Phys. 02 (2008) 019.
[5] A. Karch, E. Katz, D. T. Son, and M. A. Stephanov, Phys. Rev. D **74**, 015005 (2006).
[6] S. S. Gubser and A. Nellore, Phys. Rev. D **78**, 086007 (2008).
[7] S. S. Gubser, A. Nellore, S. S. Pufu, and F. D. Rocha, Phys. Rev. Lett. **101**, 131601 (2008).
[8] M. Bianchi, D. Z. Freedman, and K. Skenderis, J. High Energy Phys. 08 (2001) 041.
[9] K. Skenderis, Classical Quantum Gravity **19**, 5849 (2002).
[10] J. Erlich, E. Katz, D. T. Son, and M. A. Stephanov, Phys. Rev. Lett. **95**, 261602 (2005).
[11] L. Da Rold and A. Pomarol, Nucl. Phys. **B721**, 79 (2005).
[12] Z. Abidin and C. E. Carlson, Phys. Rev. D **80**, 115010 (2009).
[13] A. Ballon-Bayona, G. Krein, and C. Miller, Phys. Rev. D **96**, 014017 (2017).
[14] I. Papadimitriou, Springer Proc. Phys. **176**, 131 (2016).
[15] E. Megias and O. Pujolas, J. High Energy Phys. 08 (2014) 081.
[16] J. Bourdier and E. Kiritsis, Classical Quantum Gravity **31**, 035011 (2014).
[17] E. Kiritsis, F. Nitti, and L. S. Pimenta, Fortschr. Phys. **65**, 1600120 (2017).
[18] G. 't Hooft, Nucl. Phys. **B72**, 461 (1974).
[19] J. M. Maldacena, Int. J. Theor. Phys. **38**, 1113 (1999); Adv. Theor. Math. Phys. **2**, 231 (1998).
[20] S. S. Gubser, I. R. Klebanov, and A. M. Polyakov, Phys. Lett. B **428**, 105 (1998).
[21] E. Witten, Adv. Theor. Math. Phys. **2**, 253 (1998).
[22] Y. Kinar, E. Schreiber, and J. Sonnenschein, Nucl. Phys. **B566**, 103 (2000).
[23] J. M. Maldacena, Phys. Rev. Lett. **80**, 4859 (1998).
[24] E. Kiritsis and F. Nitti, Nucl. Phys. **B772**, 67 (2007).
[25] M. Caselle, L. Castagnini, A. Feo, F. Gliozzi, U. Gursoy, M. Panero, and A. Schafer, J. High Energy Phys. 05 (2012) 135.
[26] D. Li and M. Huang, J. High Energy Phys. 11 (2013) 088.
[27] Y. Chen and M. Huang, Chin. Phys. C **40**, 123101 (2016).
[28] I. Papadimitriou, J. High Energy Phys. 08 (2011) 119.
[29] E. Kiritsis, W. Li, and F. Nitti, Fortschr. Phys. **62**, 389 (2014).
[30] S. Janowski, F. Giacosa, and D. H. Rischke, Phys. Rev. D **90**, 114005 (2014).
[31] F. Brünner and A. Rebhan, Phys. Rev. Lett. **115**, 131601 (2015).
[32] C. F. Qiao and L. Tang, Phys. Rev. Lett. **113**, 221601 (2014).
[33] A. Pimikov, H. J. Lee, and N. Kochelev, Phys. Rev. Lett. **119**, 079101 (2017).
[34] V. Mathieu, N. Kochelev, and V. Vento, Int. J. Mod. Phys. E **E18**, 1 (2009).
[35] E. Witten, Adv. Theor. Math. Phys. **2**, 505 (1998).
[36] C. Csaki, H. Ooguri, Y. Oz, and J. Terning, J. High Energy Phys. 01 (1999) 017.
[37] R. C. Brower, S. D. Mathur, and C. I. Tan, Nucl. Phys. **B587**, 249 (2000).
[38] E. Caceres and R. Hernandez, Phys. Lett. B **504**, 64 (2001).
[39] A. Dymarsky and D. Melnikov, J. High Energy Phys. 05 (2008) 035.
[40] D. Elander and M. Piai, J. High Energy Phys. 06 (2017) 003.

[41] M. Berg, M. Haack, and W. Mueck, Nucl. Phys. **B736**, 82 (2006).
[42] M. Berg, M. Haack, and W. Mueck, Nucl. Phys. **B789**, 1 (2008).
[43] H. Boschi-Filho and N. R. F. Braga, J. High Energy Phys. 05 (2003) 009.
[44] H. Boschi-Filho, N. R. F. Braga, and H. L. Carrion, Phys. Rev. D **73**, 047901 (2006).
[45] E. Folco Capossoli and H. Boschi-Filho, Phys. Rev. D **88**, 026010 (2013).
[46] P. Colangelo, F. De Fazio, F. Jugeau, and S. Nicotri, Phys. Lett. B **652**, 73 (2007).
[47] H. Boschi-Filho, N. R. F. Braga, F. Jugeau, and M. A. C. Torres, Eur. Phys. J. C **73**, 2540 (2013).
[48] E. Folco Capossoli, D. Li, and H. Boschi-Filho, Eur. Phys. J. C **76**, 320 (2016).
[49] E. Folco Capossoli, D. Li, and H. Boschi-Filho, Phys. Lett. B **760**, 101 (2016).
[50] E. Folco Capossoli and H. Boschi-Filho, Phys. Lett. B **753**, 419 (2016).
[51] H. B. Meyer, Doctor of philosophy thesis, University of Oxford, 2005.
[52] E. S. Fraga, J. Noronha, and L. F. Palhares, Phys. Rev. D **87**, 114014 (2013).
[53] B. Lucini and M. Panero, Prog. Part. Nucl. Phys. **75**, 1 (2014).
[54] B. Lucini and M. Panero, Phys. Rep. **526**, 93 (2013).
[55] A. I. Vainshtein, V. I. Zakharov, and M. A. Shifman, Pis'ma Zh. Eksp. Teor. Fiz. **27**, 60 (1978) [JETP Lett. **27**, 55 (1978)].
[56] M. A. Shifman, A. I. Vainshtein, and V. I. Zakharov, Nucl. Phys. **B147**, 385 (1979).
[57] O. Andreev and V. I. Zakharov, Phys. Rev. D **76**, 047705 (2007).
[58] M. Campostrini, A. Di Giacomo, and Y. Gunduc, Phys. Lett. B **225**, 393 (1989).
[59] P. E. L. Rakow, *Proc. Sci.*, LAT2005 (2006) 284 [arXiv: 0510046].
[60] J. de Boer, E. P. Verlinde, and H. L. Verlinde, J. High Energy Phys. 08 (2000) 003.
[61] T. Gherghetta, J. I. Kapusta, and T. M. Kelley, Phys. Rev. D **79**, 076003 (2009).
[62] M. Jarvinen and E. Kiritsis, J. High Energy Phys. 03 (2012) 002.
[63] U. Gursoy, E. Kiritsis, L. Mazzanti, and F. Nitti, J. High Energy Phys. 05 (2009) 033.
[64] A. S. Miranda, C. A. Ballon Bayona, H. Boschi-Filho, and N. R. F. Braga, J. High Energy Phys. 11 (2009) 119.
[65] R. C. Brower, J. Polchinski, M. J. Strassler, and C. I. Tan, J. High Energy Phys. 12 (2007) 005.
[66] A. Ballon-Bayona, R. Carcassés Quevedo, M. S. Costa, and M. Djurić, Phys. Rev. D **93**, 035005 (2016).
[67] R. Nally, T. G. Raben, and C. I. Tan, J. High Energy Phys. 11 (2017) 075.
[68] A. Ballon-Bayona, R. Carcassés Quevedo, and M. S. Costa, J. High Energy Phys. 08 (2017) 085.
[69] P. Breitenlohner and D. Z. Freedman, Phys. Lett. **115B**, 197 (1982).